

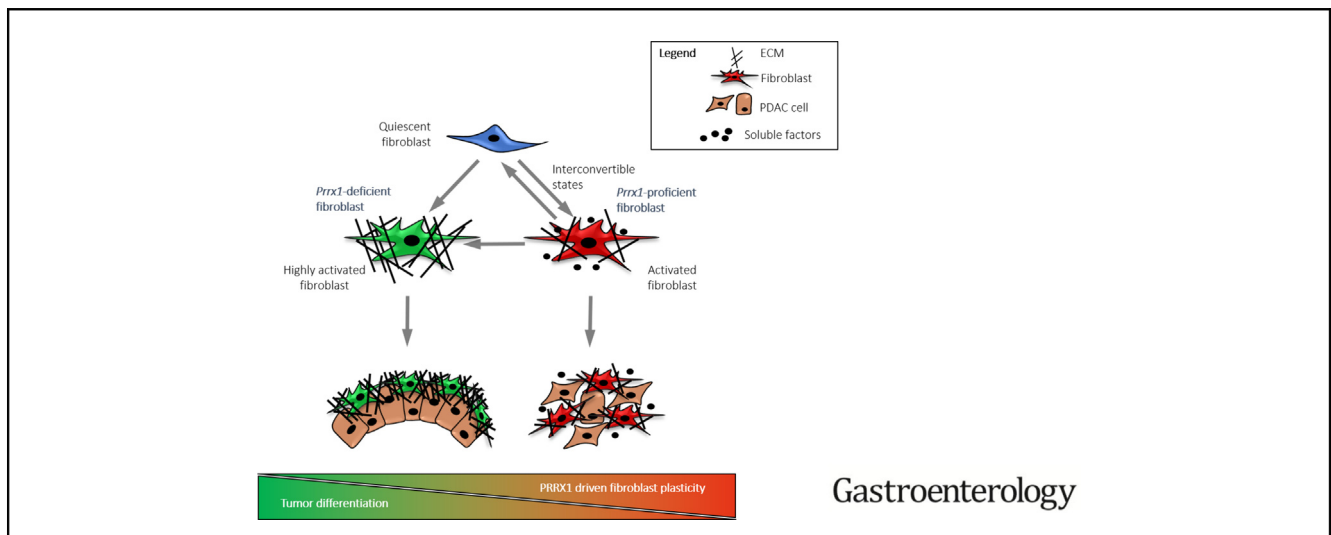
BASIC AND TRANSLATIONAL—PANCREAS

Mesenchymal Plasticity Regulated by *Prrx1* Drives Aggressive Pancreatic Cancer Biology



Karin Feldmann,¹ Carlo Maurer,¹ Katja Peschke,¹ Steffen Teller,² Kathleen Schuck,^{1,2} Katja Steiger,^{3,4,5} Thomas Engleitner,^{1,5} Rupert Öllinger,^{1,5} Alice Nomura,¹ Nils Wirges,^{3,4} Aristeidis Papargyriou,^{1,6} Rim Sabrina Jahan Sarker,^{3,4} Raphela Aranie Ranjan,¹ Zahra Dantes,¹ Wilko Weichert,^{3,4,5} Anil K. Rustgi,⁷ Roland M. Schmid,^{1,5} Roland Rad,^{1,5} Günter Schneider,^{1,5} Dieter Saur,^{1,5} and Maximilian Reichert^{1,5}

¹Klinik und Poliklinik für Innere Medizin II, Klinikum rechts der Isar, Technical University of Munich, Munich, Germany; ²Department of Surgery, Klinikum rechts der Isar, Technical University of Munich, Munich, Germany; ³Institute of Pathology, Technical University of Munich, Munich, Germany; ⁴Comparative Experimental Pathology, Technical University of Munich, Munich, Germany; ⁵German Cancer Consortium, Partner Site Munich, Germany; ⁶Institute of Stem Cell Research, Helmholtz Center for Health and Environmental Research Munich, Neuherberg, Germany; and ⁷Herbert Irving Comprehensive Cancer Center, Columbia University Irving Medical Center, Columbia University, New York, New York



Gastroenterology

See Covering the Cover synopsis on page 2.

BACKGROUND & AIMS: Pancreatic ductal adenocarcinoma (PDAC) is characterized by a fibroblast-rich desmoplastic stroma. Cancer-associated fibroblasts (CAFs) have been shown to display a high degree of interconvertible states including quiescent, inflammatory, and myfibroblastic phenotypes; however, the mechanisms by which this plasticity is achieved are poorly understood. Here, we aim to elucidate the role of CAF plasticity and its impact on PDAC biology. **METHODS:** To investigate the role of mesenchymal plasticity in PDAC progression, we generated a PDAC mouse model in which CAF plasticity is modulated by genetic depletion of the transcription factor *Prrx1*. Primary pancreatic fibroblasts from this mouse model were further characterized by functional in vitro assays. To characterize the impact of CAFs on tumor differentiation and response to chemotherapy, various

coculture experiments were performed. In vivo, tumors were characterized by morphology, extracellular matrix composition, and tumor dissemination and metastasis. **RESULTS:** Our in vivo findings showed that *Prrx1*-deficient CAFs remain constitutively activated. Importantly, this CAF phenotype determines tumor differentiation and disrupts systemic tumor dissemination. Mechanistically, coculture experiments of tumor organoids and CAFs showed that CAFs shape the epithelial-to-mesenchymal phenotype and confer gemcitabine resistance of PDAC cells induced by CAF-derived hepatocyte growth factor. Furthermore, gene expression analysis showed that patients with pancreatic cancer with high stromal expression of *Prrx1* display the squamous, most aggressive, subtype of PDAC. **CONCLUSIONS:** Here, we define that the *Prrx1* transcription factor is critical for tuning CAF activation, allowing a dynamic switch between a dormant and an activated state. This work shows that *Prrx1*-mediated CAF plasticity has significant impact on PDAC biology and therapeutic resistance.

Keywords: Cancer-Associated Fibroblasts; Myofibroblasts; Pancreatic Ductal Adenocarcinoma; Extracellular Matrix Proteins.

Pancreatic ductal adenocarcinoma (PDAC) is a complex disease that is no longer viewed as purely an accumulation of mutations in cells. Instead, the PDAC microenvironment influences tumor cell initiation, progression, and metastasis. The tumor microenvironment (TME) comprises immune cells, extracellular matrix (ECM) proteins, soluble factors, neurons, endothelial cells, adipocytes, and cancer-associated fibroblasts (FBs) (CAF).^{1–3} CAFs represent a heterogeneous cell population with mesodermal origin,⁴ and pancreatic stellate cells (PSCs) are the most studied subtype of this population. Through extrinsic cues, quiescent PSCs differentiate into α -smooth muscle actin (α -SMA)-expressing activated PSCs, which are proliferative and migratory, as well as sources of ECM proteins and active soluble factors.^{5–7} However, activated FBs also provide tumor-supporting effects through paracrine signaling, favoring tumor growth and metastatic dissemination.^{8–10}

Because of the central role of CAFs within the TME, novel therapeutic targeting strategies were developed. For example, in genetically engineered mouse models, reprogramming of activated FBs into quiescent PSCs by vitamin D receptor activation suppresses a tumor-promoting secretome, resulting in improved outcomes.¹¹ An approach to enhance drug delivery in a mouse model of PDAC is the inhibition of Smo (Hedgehog) signaling pathway, which resulted in a decrease of proliferation of FB and collagen content and an increase of vascularization.¹² However, the coadministration of IPI-926 (a Hedgehog inhibitor) to suppress CAF protumorigenic functions and gemcitabine resulted in a failed phase 2 clinical trial.¹³ As a result, follow-up studies were conducted in which targeting α -SMA⁺ myofibroblasts or *Shh* deletion in pancreatic cancer cells in genetically engineered mouse models suggested a protective role of the stroma.^{14,15} Another strategy to overcome CAF-mediated chemoresistance is to break down the ECM, for example, through the degradation of hyaluronic acid^{16,17} or by using anti-angiogenic therapies.¹⁸ Unfortunately, phase 3 of the clinical trial using PEGPH20 in combination with gemcitabine and nab-paclitaxel failed, highlighting the need to better understand the role of stroma.¹⁹

These protumorigenic and antitumorigenic functions might be due to CAF heterogeneity.⁶ Öhlund et al.²⁰ identified 2 different groups of FBs and coined the terms *inflammatory CAFs* (iCAFs) and myofibroblastic CAFs (myCAFs).²⁰ iCAFs express inflammatory markers, like interleukin (IL) 6 and leukemia inhibitory factor, which promote tumor progression and systemic effects, such as immune suppression.^{20,21} Conversely, myCAFs exhibit a tumor-restraining function.^{14,15,20} Both CAF subtypes represent interconvertible states, underscoring the need to understand plasticity in FBs.²⁰

The paired-related homeobox 1 (Prrx1) transcriptional factor was identified as a driver of cellular plasticity during

WHAT YOU NEED TO KNOW

BACKGROUND AND CONTEXT

The transcriptional factor Prrx1 is a plasticity driver during pancreatic ductal development, pancreatitis and carcinogenesis within the epithelial compartment. Recently, it was shown that cancer-associated fibroblasts also display pronounced cellular plasticity leading to distinct phenotypes impacting differently upon tumor biology. Here, we investigate the role of Prrx1 in pancreatic cancer-associated fibroblasts (CAFs).

NEW FINDINGS

Genetic *Prrx1* deletion forces CAFs into a highly activated state resulting in an increased ECM deposition. This specific CAF phenotype leads to improved tumor differentiation, increased sensitivity towards chemotherapeutic treatment and disrupts systemic tumor dissemination.

LIMITATIONS

Although varying stromal Prrx1 gene expression levels correlate with distinct human pancreatic cancer subtypes confirming our results, more work is needed using human model systems.


IMPACT

The *Prrx1* transcription factor is essential for CAF plasticity and impacts upon PDAC biology and therapeutic resistance. Our findings identify CAF plasticity as potential therapeutic target in PDAC.

pancreatic ductal development, acinar-to-ductal metaplasia, and carcinogenesis.²² In addition, Prrx1 is a key regulator of epithelial-to-mesenchymal transition (EMT) and metastatic colonization in PDAC.²³ These processes are regulated by isoform switching of Prrx1. The isoform Prrx1b promotes EMT through up-regulation of the hepatocyte growth factor (HGF), whereas Prrx1a regulates tumor differentiation and metastatic outgrowth.²³

Here, we identified high Prrx1 expression levels in the PDAC stroma. Importantly, we found that high stromal expression levels of Prrx1 are associated with the squamous subtype, whereas low stromal Prrx1 expression is found in classical PDAC, thereby indicating a potential functional role of Prrx1 in CAFs. Consequently, we developed a conditional

Abbreviations used in this paper: 3D, 3-dimensional; α -SMA, α -smooth muscle actin; CAF, cancer-associated fibroblast; ECM, extracellular matrix; EpCAM, epithelial cell adhesion molecule; ELISA, enzyme-linked immunosorbent assay; EMT, epithelial-mesenchymal transition; iCAF, inflammatory cancer-associated fibroblast; FB, fibroblast; GFP, green fluorescent protein; HGF, hepatocyte growth factor; IF, immunofluorescence; IHC, immunohistochemistry; IL, interleukin; myCAF, myofibroblastic cancer-associated fibroblast; PanIN, pancreatic intraepithelial neoplasia; PDAC, pancreatic ductal adenocarcinoma; Prrx1, paired related homeobox 1; PSC, pancreatic stellate cell; RNA-seq, RNA sequencing; SPARC, secreted protein acidic and cysteine rich; TAM, tamoxifen; TGF, transforming growth factor; TME, tumor microenvironment.

 Most current article

© 2021 by the AGA Institute. Published by Elsevier Inc. This is an open access article under the CC BY-NC-ND license (<http://creativecommons.org/licenses/by-nc-nd/4.0/>).

0016-5085

<https://doi.org/10.1053/j.gastro.2020.09.010>

knockout allele of *Prrx1* to specifically ablate *Prrx1* in FBs, both in vitro and in vivo. Mechanistically, we describe that loss of *Prrx1* mediates CAF activation and leads to increased amounts of ECM, improved tumor differentiation, fewer circulating tumor cells, and reduced metastasis. At the same time, *Prrx1* in CAFs promotes EMT and chemotherapeutic resistance in tumor cells through paracrine HGF signaling.

Materials and Methods

Experimental Animals

All animal experiments and care were in accordance with the guidelines of institutional committees and approved by the local authority, Regierung von Oberbayern, project number 55.2-1-54-2532-1-2017.

Three-Dimensional Organoid Culture and Immunofluorescence

Three-dimensional (3D) pancreatic cell culture was performed as previously described.^{22,24}

Tissue Immunohistochemical/Immunofluorescence Staining

Immunohistochemistry (IHC) and immunofluorescence (IF) staining were carried out as described previously²³ and as detailed in [Supplementary Experimental Procedures](#).

Quantification of Single-Color Immunofluorescence Signals

The quantification protocol was developed by Koushik Das, MD (Washington University School of Medicine, St. Louis, MO).²⁵

Statistical Analysis

Data are presented as mean \pm standard error of the mean. For all in vitro and in vivo experiments, statistical analyses were performed using the Student *t* test except where otherwise noted. Significance was noted as $P < .05$.

Data Availability

The authors declare that all data supporting the results of this study are available within the article or its supplementary information files. Please also see the [Supplementary Experimental Procedures](#) for details.

Results

Prrx1 Is Highly Expressed in Cancer-Associated Fibroblasts

PRRX1 has been described as a regulator of pancreatic epithelial plasticity.^{22,23} It is apparent in other human cancers, for example, in colon, esophageal, and lung cancer, that PRRX1 expression is not restricted to tumor cells but is also expressed in the tumor stroma.^{26,27} Histologic analysis of PRRX1 expression in murine (*Pdx1-Cre;Kras^{G12D/+};Ink4/ARF^{fl/+}*) and human PDAC showed that, indeed, PRRX1 expression is not limited to the

tumor cell compartment but is also found in the tumor stroma, including CAFs ([Figure 1A and B](#)). To differentiate stromal and tumor cell-derived gene expression (based on species differences), Nicolle et al²⁸ performed RNA profiling of 30 xenograft bulk tumors from patients with PDAC.²⁸ In this data set, *Prrx1* is a highly up-regulated in the stroma ([Figure 1C](#)). Gene expression analysis of primary human cell cultures showed that the *PRRX1* level is significantly higher in CAFs compared to PDAC cells ([Figure 1D](#)). In addition, we isolated pancreatic ductal cells, FBs, and PSCs from *C57BL/6* mice, pancreatic intraepithelial neoplasia (PanIN) cells and PanIN-associated FBs from *Pdx1-Cre;Kras^{G12D/wt}* mice as well as PDAC cells from *p48-Cre;FSF-Kras^{G12D}* mice and CAFs from *p48-Cre;LSL-Kras^{G12D/+};Tgfb β 2^{fl/fl}* mice ([Supplementary Table 1](#)). Gene expression analysis of these cell lines showed that both *Prrx1* splice variants are significantly up-regulated in FBs compared to ductal cells ([Figure 1E and F](#)).

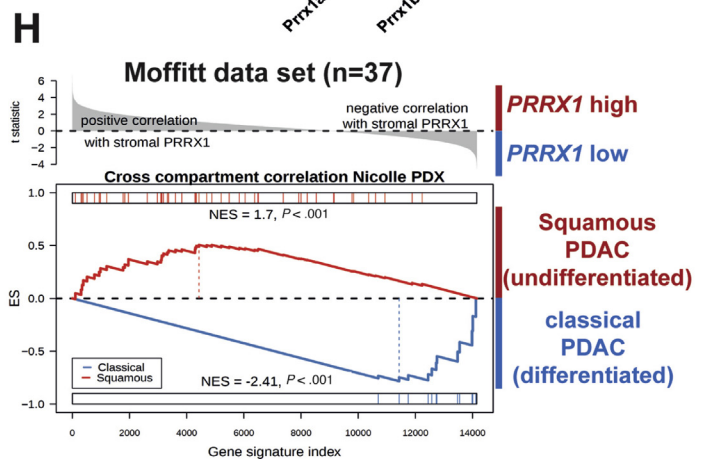
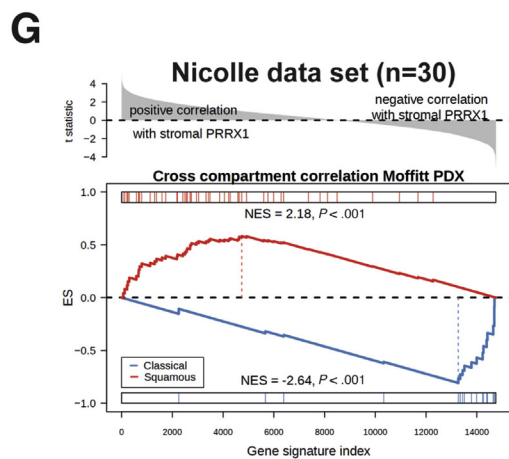
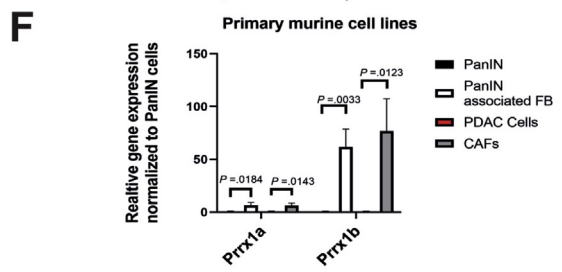
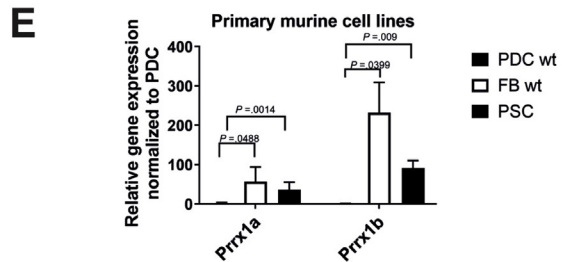
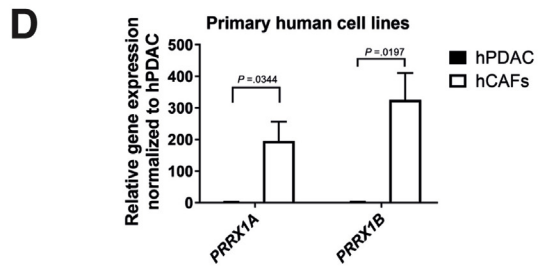
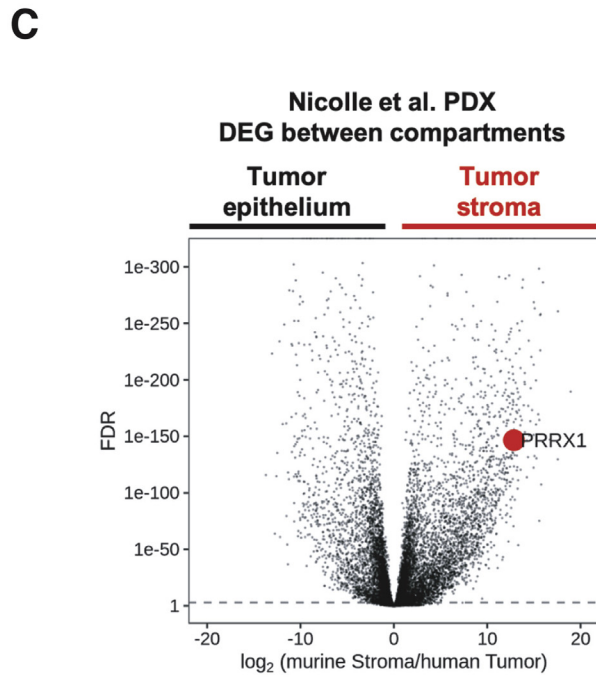
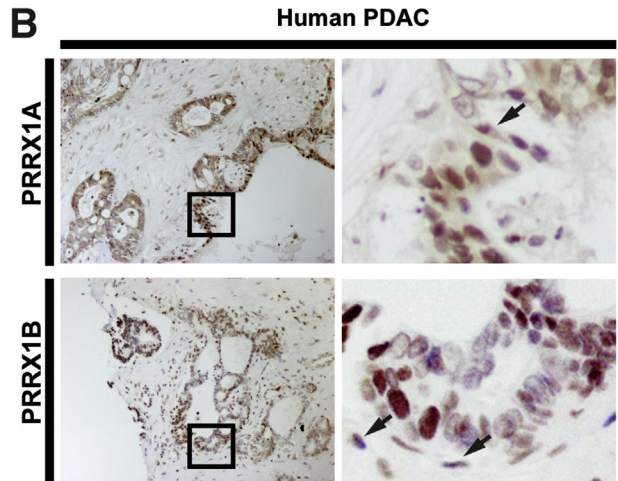
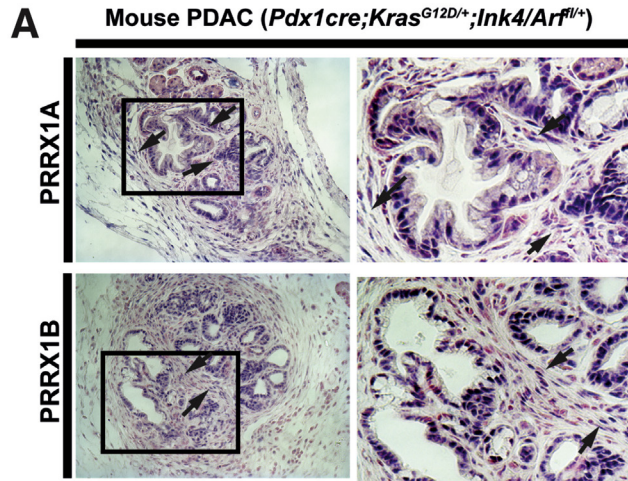
To corroborate these findings, we analyzed published single-cell RNA-sequencing (RNA-seq) data sets in mouse and human PDACs. Analyses of data by Elyada et al²⁹ showed that iCAF and myCAF express the highest *Prrx1* levels compared to the ductal cells and antigen-presenting CAFs in mice ([Supplementary Figure 1A](#)).²⁹ In the human data set by Peng et al,³⁰ PRRX1 expression is low in the ductal compartment compared to tumor FBs ([Supplementary Figure 1B](#)).³⁰ In addition, PRRX1 is highly expressed in human myCAFs but also in iCAFs ([Supplementary Figure 1C](#)).

These data indicate that *Prrx1* is highly expressed in the stromal compartment of PDAC, especially in FBs.

Stromal PRRX1 Expression Correlates With the Squamous Subtype in Human Pancreatic Ductal Adenocarcinoma

Multiple genomics studies have identified various molecular subtypes of PDAC, but The Cancer Genome Atlas Research Network reported that most PDACs can be classified into 2 major subtypes based on cancer cell autonomous properties: the classical/pancreatic progenitor subtype and the basal-like/squamous subtype.³¹⁻³⁴ The squamous subtype confers a poorer prognosis, with a median survival time significantly shorter than that observed in the classical/progenitor subtype.^{31,33}

To evaluate whether stromal PRRX1 influences the molecular subtype of PDAC, a cross-compartment correlation analysis was performed based on species-specific RNA-seq data obtained from Moffitt et al³¹ (xenografts, $n = 37$) and Nicolle et al²⁸ (xenografts, $n = 30$) ([Figure 1G and H](#)). Importantly, our analyses showed that stromal PRRX1 correlates significantly with the squamous subtype. Conversely, low PRRX1 level correlates with the classical subtype. These results indicate that stromal expressed PRRX1 might shape tumor differentiation, which is an independent prognostic factor for patient survival across all pancreatic tumor stages.



Prrx1-Deficient Fibroblasts Display an Activated Phenotype In Vitro

To investigate the functional role of *Prrx1* in FBs and since global *Prrx1* knockout is lethal,^{35,36} we generated a conditional loss-of-function *Prrx1* allele. To achieve compartment-specific ablation of *Prrx1*, we placed the *Prrx1*^{fl/fl} allele under the control of the *Sm22-Cre*^{ERT} promoter (*Sm22-Cre*^{ERT}, a knock-in to the smooth muscle protein 22 alpha [SM22] locus, targets FBs³⁷). Interestingly, the *Sm22* gene (*Tagln*) is highly expressed in the myCAF subpopulation (Supplementary Figure 1D). To visualize recombination, a fluorescent reporter allele was introduced (*Rosa26*^{mTmG}).³⁸ To characterize the expression pattern of *Sm22-Cre*^{ERT}; *Rosa26*^{mTmG}, IF staining was performed (Supplementary Figure 2A and B), showing efficient recombination of FBs as well as smooth muscle tissue upon tamoxifen (TAM) administration. Orthotopic (intra-pancreatic) implantation of PDAC cells showed an increased presence of *Sm22-Cre*^{ERT}-positive cells in the pancreas (Supplementary Figure 2C). Additionally, α -SMA staining confirmed that CAFs were targeted successfully by the *Sm22-Cre*^{ERT} (Supplementary Figure 2D). We next generated primary pancreatic FB cell lines from *Sm22-Cre*^{ERT}; *Prrx1*^{fl/fl} mice (Supplementary Figure 3A and B). After TAM treatment, we analyzed RNA and protein levels, confirming in vitro recombination (Supplementary Figure 3E and F). Flow cytometry showed an in vitro recombination efficiency of approximately 90% (Supplementary Figure 3D). In addition to quantitative gene expression analysis, PRRX1 staining confirmed significant *Prrx1* knockdown after TAM treatment. IF staining for FB markers such as α -SMA, vimentin, Platelet-derived growth factor receptor- α , and FB-activating protein (Supplementary Figure 3B and C) indicated a myofibroblast identity.³⁹

To determine whether *Prrx1* can alter the activation status of FBs, α -SMA staining was performed (Figure 2A). Quantification of α -SMA staining showed that *Prrx1*-deficient FBs expressed higher α -SMA levels compared to *Prrx1*-proficient FBs (Figure 2B). To challenge the correlation of *Prrx1* and α -SMA, we asked whether the effect of *Prrx1*-depletion on α -SMA expression can be rescued upon reinduction of *Prrx1* isoform expression. For this purpose, we used mouse embryonic FBs from wild-type or global *Prrx1*-knockout mice (*Prrx1* KOFB)⁴⁰ and stable transduced the *Prrx1* KOFB with either *Prrx1a* (*Prrx1a* FB) or *Prrx1b* (*Prrx1b* FB). Interestingly, *Prrx1b* but not *Prrx1a* is able to decrease α -SMA expression on

the messenger RNA (mRNA) and protein levels (Supplementary Figure 4A–D).

Besides α -SMA expression, we next determined the activation status of FBs functionally. *Prrx1*-proficient and -deficient FBs displayed no differences in proliferation (Supplementary Figure 4E). To assess collagen secretion—a key feature of activated FBs—we quantified newly synthesized collagen in *Prrx1*-proficient and -deficient FBs lysates using a colorimetric dye-binding assay (Sircol soluble collagen assay Biocolor Ltd, County Antrim, United Kingdom) (Figure 2C). *Prrx1*-deficient FBs (+TAM) expressed increased amounts of collagen compared to *Prrx1*-proficient (–TAM) (Figure 2C). Because cellular adhesion is essential for the migration of activated FBs, because it links the cytoskeleton and extracellular matrix, we determined the effect of *Prrx1* on cellular adhesion as well as migration. *Prrx1*-deficient FBs display a higher adhesion capacity on collagen I-coated surfaces (Figure 2D). Furthermore, we performed a 3D migration assay to determine the *Prrx1*-regulated ability of FBs to migrate toward tumor cells (Figure 2E). After 16 hours, we observed an increased migration of recombined *Prrx1*^{fl/fl} FBs toward tumor cells (Figure 2F). Time-lapse microscopy (48 hours) showed that recombined *Prrx1*^{fl/fl} FBs migrated faster (Euclidean distance) and more directed toward tumor cells (forward migration index) (Figure 2G and H).

In summary, these data indicate that loss of *Prrx1* leads to notable FB activation, including α -SMA expression, collagen production, and cellular migration.

Altering *Prrx1* Expression in Fibroblasts Leads to Changes in the Tumor-Associated Extracellular Matrix In Vivo

Next, we assessed the in vivo significance of *Prrx1* deficiency in FBs during tumor progression. For this, we chose the *Sm22-Cre*^{ERT}; *Prrx1*^{fl/fl}; *Rosa26*^{mTmG} mouse model. Administration of TAM to 6–8-week-old mice had no effect on organ development and architecture (pancreas, liver, intestine, and lung) (Supplementary Figure 5A–C). Also, the presence of spontaneous recombination of *Sm22-Cre*^{ERT} without TAM administration was excluded by flow cytometry (Supplementary Figure 5B). To study further *Prrx1* in CAFs, tumor cells (8025 PPT cell line isolated from a *p48-Cre*; *FSF-Kras*^{G12D} mouse in a C57BL/6 background) were implanted in the tail of the pancreas of *Sm22-Cre*^{ERT}; *Prrx1*^{fl/fl} (\pm TAM) mice with an age of 12 weeks (Supplementary

Figure 1. PRRX1 is highly expressed in the stromal compartment of PDACs. (A) PRRX1A and PRRX1B IHC in mouse sections with the indicated genotype. (B) PRRX1A and PRRX1B IHC in human sections. The black arrows indicate PRRX1-positive stromal cells. (C) Volcano plot illustrating the differential gene expression analysis between the stromal and epithelial compartments of patient-derived xenografts profiled by Nicolle et al.²⁸ Stromal PRRX1 expression by far exceeds epithelial expression (log₂ fold change, 12.9; false discovery rate, 2.6E3147). (D) qPCR analysis of PRRX1A and PRRX1B expression in primary human cell lines (3 tumor cell lines and 4 FB cell lines), unpaired Student *t* test. (E) qPCR analysis of *Prrx1a* and *Prrx1b* expression in primary murine cell lines isolated from wild-type mice (3 cell lines of each cell type: pancreatic ductal cells, FBs, and PSCs), unpaired Student *t* test. (F) qPCR analysis of *Prrx1a* and *Prrx1b* expression in primary murine cell lines (3 PanIN cell lines, 3 PanIN-associated FB cell lines, 1 CAF cell line), unpaired Student *t* test. (G) Cross-compartment correlation based on data from Moffitt et al.³¹ (H) Cross-compartment correlation based on data from Nicolle et al.²⁸ DEG, differentially expressed genes; FDR, false discovery rate; h, human; PDX, patient-derived xenografts; qPCR, quantitative polymerase chain reaction; wt, wild type.

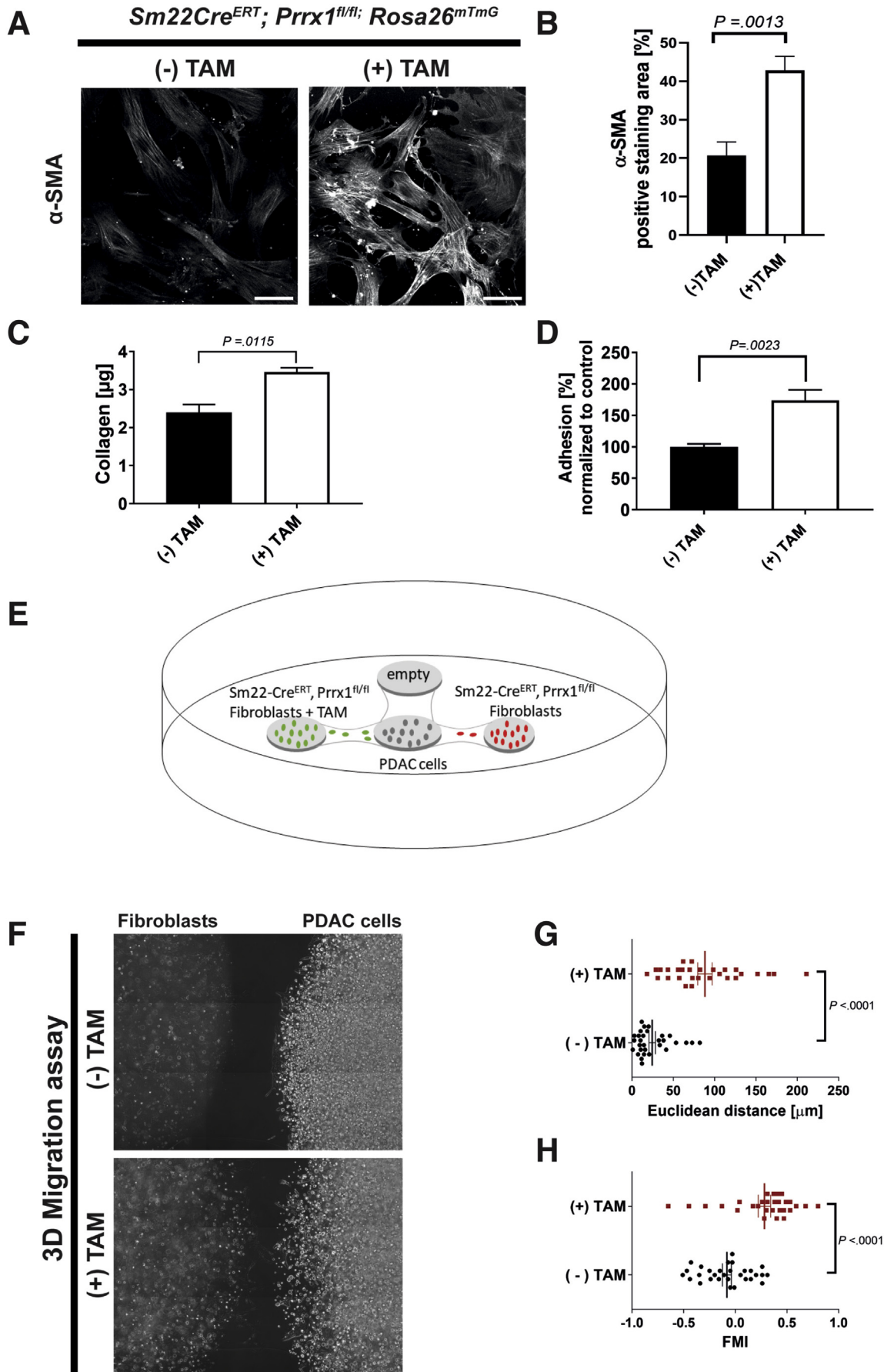


Figure 6A and B). To assess compartment-specific recombination in CAFs, we used the *R26^{mTmG}* reporter allele and stained for the CAF marker α -SMA. Colocalization of green fluorescent protein (GFP) and α -SMA indicates recombination within CAFs, an observation validated by the detection of GFP-positive cells in the pancreas via flow cytometry (Supplementary Figure 6C, D, and I). In most cases, the pancreas had been completely penetrated by the tumor, and analysis of pancreata showed a decrease in PRRX1 expression in CAFs (Supplementary Figure 6F and G). There was no difference detectable in survival between both experimental groups; however, this is likely due to the extremely fast tumor progression in this aggressive orthotopic model (Supplementary Figure 6E).

To investigate the relationship between *Prrx1* ablation in CAFs and ECM composition, we analyzed the expression of different stromal markers at the 2-week timepoint ($n = 3$ per group). We detected an increase in total ECM content, particularly an increase in fibrillar collagen (Elastica van Gieson and Picro Sirius Red staining) and fibronectin in the *Prrx1*-knockout CAFs (Figure 3A). In addition, secreted protein acidic and rich in cysteine (SPARC) expression was increased significantly in *Prrx1*-knockout CAFs (Figure 3B and C). Because FBs are the major source of collagen I,⁴¹ we quantified the collagen I-positive areas and observed a significant increase in collagen I in the ECM (Figure 3B and D). We also noted an increase in the number of α -SMA-positive cells in the *Prrx1*-knockout CAF tumors compared to wild-type CAF tumors (Figure 3B and E).

To validate our in vivo findings in an endogenous mouse model, we crossed *Sm22-Cre^{ERT};Prrx1^{fl/fl}* mice with *KF* mice (*Pdx-Flp;FSF-Kras^{G12D}*) (Supplementary Figure 7A) and *KPF* mice (*Pdx-Flp;FSF-Kras^{G12D};p53^{flr/wt}*) (Supplementary Figure 8A), resulting in *Pdx-Flp;FSF-Kras^{G12D};Sm22-Cre^{ERT}Prrx1^{fl/fl}* (*KFSPrrx1^{fl/fl}*) and *Pdx-Flp;FSF-Kras^{G12D/+};p53^{flr/+};Sm22-Cre^{ERT};Prrx1^{fl/fl}* (*KPFSPrrx1^{fl/fl}*) animals. The dual-recombinase system allows us to genetically drive pancreatic tumorigenesis and to target *Sm22-Cre^{ERT}*-positive FBs independently.⁴² Similar to the transplantation model, we observed an increase of α -SMA⁺ and vimentin⁺ cells in tumors with *Prrx1*-knockout FBs as well as an increase of collagen and SPARC in the tumor-associated ECM (Supplementary Figure 7B–F and Supplementary Figure 8B–D). These data underscore the role of *Prrx1* tuning FB activation and remodeling of the ECM in vivo.

To analyze the impact of *Prrx1* on immune cell infiltration of the stroma, tissue sections were immunophenotyped. Interestingly, the orthotopic implantation model with *Prrx1*-deficient FBs as well as the endogenous *KFSPrrx1^{fl/fl}* model showed a significant increase in CD3⁺, CD8⁺ and CD4⁺ T

cells and B cells, as well as macrophages and dendritic cells (Figure 3F and Supplementary Figure 7G) compared to the *Prrx1*-proficient controls. These data indicate that the *Prrx1*-proficient CAFs might shape an immunosuppressive TME.

Prrx1 Deficiency in Cancer-Associated Fibroblasts Improves Tumor Differentiation and Decreases Systemic Dissemination In Vivo

We next analyzed tumor grading of orthotopically implanted pancreatic tumors. Grading of 21 tumors showed that tumors with *Prrx1*-deficient CAFs (+TAM) were more differentiated (G2, 40%; G3, 60%) compared to controls (-TAM) (G2, 27%; G3, 73%) (Figure 4A and B). Additionally, histology of the *KF* and *KFSPrrx1^{fl/fl}* mice at the ages of 12 and 18 months confirmed that carcinogenesis in *KFSPrrx1^{fl/fl}* is decelerated, only showing acinar-to-ductal metaplasia/PanIN formation, whereas the *KF* mice display G1 and G2 tumors at the same timepoints (Supplementary Figure 9A–D).

To test whether tumor differentiation has an impact on tumor cell dissemination and metastasis, we quantified epithelial cell adhesion molecule (EpCAM)⁺ cells within the blood stream as well as the number of liver and lung metastases in the orthotopic model system. Interestingly, flow cytometry analyses showed a decreased amount of circulating EpCAM⁺ cells in TAM-treated *Sm22-Cre^{ERT};Prrx1^{fl/fl}* mice (Figure 4C). Importantly, in mice harboring *Prrx1*-deficient CAFs, the metastasis phenotype was completely abrogated (Figure 4C–E).

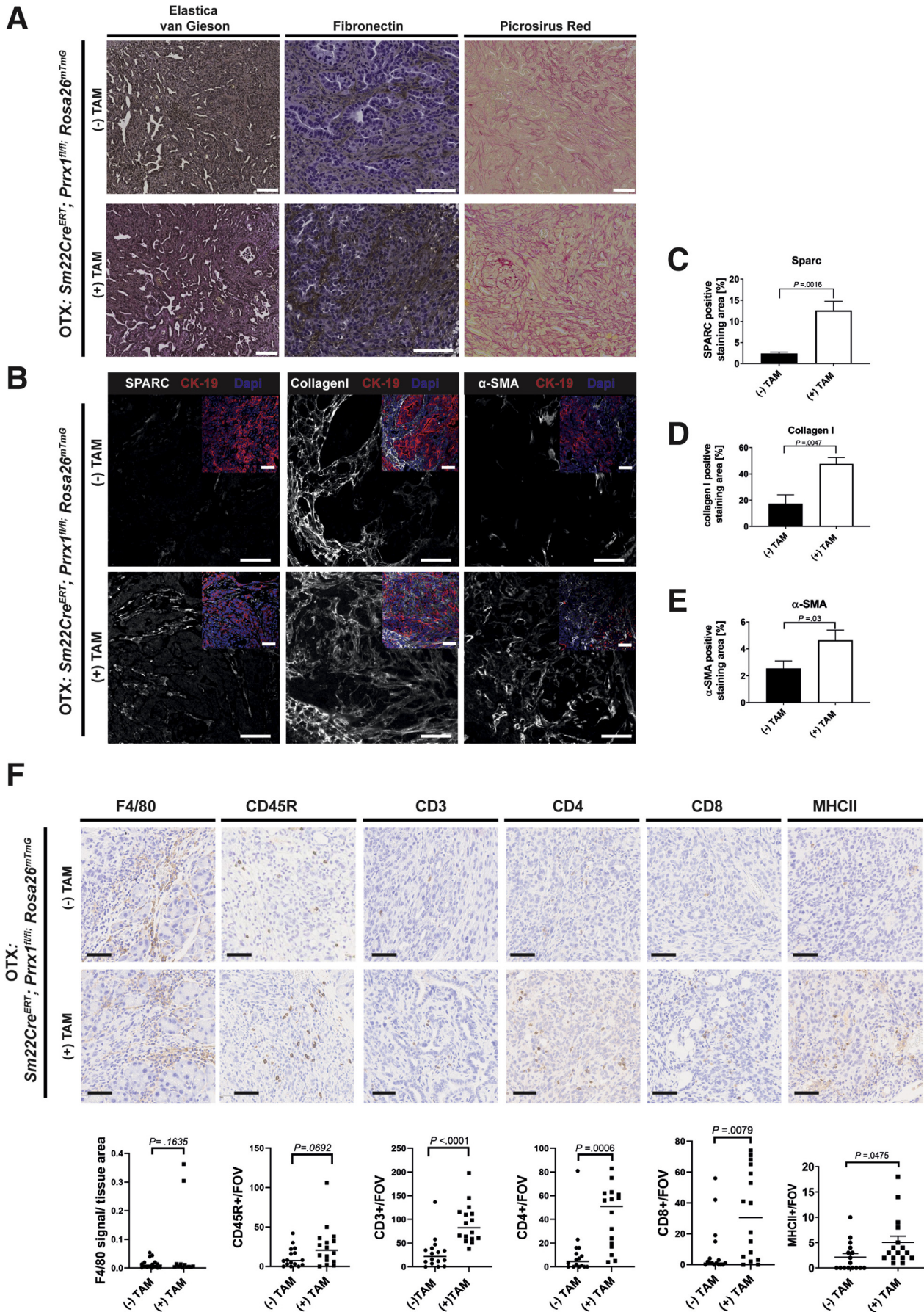
These data indicate that *Prrx1* in CAFs controls tumor architecture as well as systemic tumor dissemination and metastasis.

Prrx1-Deficient Fibroblasts Display a Myofibroblastic Cancer-Associated Fibroblast Identity and Attenuated Plasticity In Vitro

We next aimed to shed light on the impact of *Prrx1* on CAF identity. Recently, Öhlund et al²⁰ identified 2 CAF subtypes, iCAF and myCAF, based on mRNA profiling. Analyzing the data by Öhlund et al showed decreased *Prrx1* expression as well as *Prrx1*-regulated genes (*Twist1*, *Hgf*, *Tnc*) in myCAFs, whereas *Vimentin*, *Acta2*, *Sparc*, and *Col1a1* were increased (Figure 5A).^{23,26,43,44} In line with these results, we have observed increased expression levels of VIM, α -SMA, SPARC, and COL1A1 in *Prrx1*-deficient FBs, indicating a myCAF identity (Figure 3B and Supplementary Figure 7B).

In addition, we performed mRNA sequencing of *Prrx1*-proficient and -deficient FBs (Supplementary Figure 10A and B). We observed a significant enrichment of gene sets

Figure 2. *Prrx1* ablation of *Sm22-Cre^{ERT};Prrx1^{fl/fl};Rosa26^{mTmG}* FBs leads to a highly activated phenotype in vitro. (A) Representative IF staining of α -SMA (scale bar, 50 μ m) plus a semiquantitative processed image of α -SMA staining. (B) Quantification of α -SMA⁺ staining area of FBs, unpaired Student *t* test; ****P* = .008. (C) Determination of collagen content in cell lysate of FBs, unpaired Student *t* test (3 FB cell lines and 1 PSC line were used). (D) Quantification of adhesion assay via MTT, unpaired Student *t* test (3 FB cell lines were used). (E) Schematic diagram of the 3D migration assay. (F) Light microscopy pictures 16 hours after start of the experiment; scale bar, 100 μ m. Tumor cells were seeded to the left and FBs to the right. (G) Diagram shows a forward migration index of $n = 30$ per group, unpaired Student *t* test; *****P* < .0001. (H) Euclidian distance indicates how fast FBs migrate forward; $n = 30$ per group, unpaired Student *t* test; *****P* < .0001



involved in ECM secretion and remodeling as well as EMT (this gene set contains matrix-related genes) in *Prrx1*-deficient FBs (Supplementary Figure 10A). Specifically, we found an up-regulation of ECM candidates such as *Fn1*, *Sparc*, *Col1a1*, *Col3a1*, and *Lamc1*, confirming our in vitro and in vivo findings. In contrast, *Prrx1*-proficient FBs display an enrichment of gene sets involved in RNA processing, cell cycle, and unfolded protein response (Supplementary Figure 10B).

CAF identity has been shown to be dynamic. Activated myCAFs are able to revert back to a quiescent state by placing them into Matrigel [Corning, NY].^{20,45} To investigate *Prrx1*-driven CAF plasticity, *Prrx1*-proficient and *Prrx1*-deficient FBs were embedded in Matrigel (Figure 5B). Interestingly, gene expression analysis of FBs in Matrigel showed that FBs lacking *Prrx1* remain in their activated state characterized by ECM organization, ECM disassembly, activation of matrix metalloproteases, and collagen formation enriched gene sets (Supplementary Figure 11A). In contrast, *Prrx1*-proficient FBs are able to revert back to a quiescent state characterized by enriched gene sets for metabolism and the triglyceride metabolic process (Supplementary Figure 11B).

Indeed, immunofluorescence staining for α -SMA and phalloidin confirmed that recombined *Prrx1*^{f/f} FBs are unable to revert to their quiescent state when cultured in Matrigel, retaining their activated and morphologic phenotype (Figure 5C, upper panel, and D). Additionally, *Prrx1*-deficient FBs contain fewer lipid droplets compared to controls (Supplementary Figure 12A). The addition of transforming growth factor (TGF) β , which promotes a myofibroblastic phenotype,²⁵ is able to override these differences and forces FBs into an activated state in Matrigel (Figure 5C, lower panel, and E). Conversely, supplementing the media with calcipotriol, a potent and nonhypercalcemic vitamin D analog, which is able to revert activated FBs into a quiescent state,¹¹ showed reduced lipid droplet formation in FBs lacking *Prrx1* (TAM+) compared to controls (Supplementary Figure 12A). These data illustrate that *Prrx1* mediates FB plasticity.

Prrx1-Expressing Fibroblasts Stimulate Hepatocyte Growth Factor Signaling and Thereby Promote Epithelial-Mesenchymal Transition in Pancreatic Tumor Cells

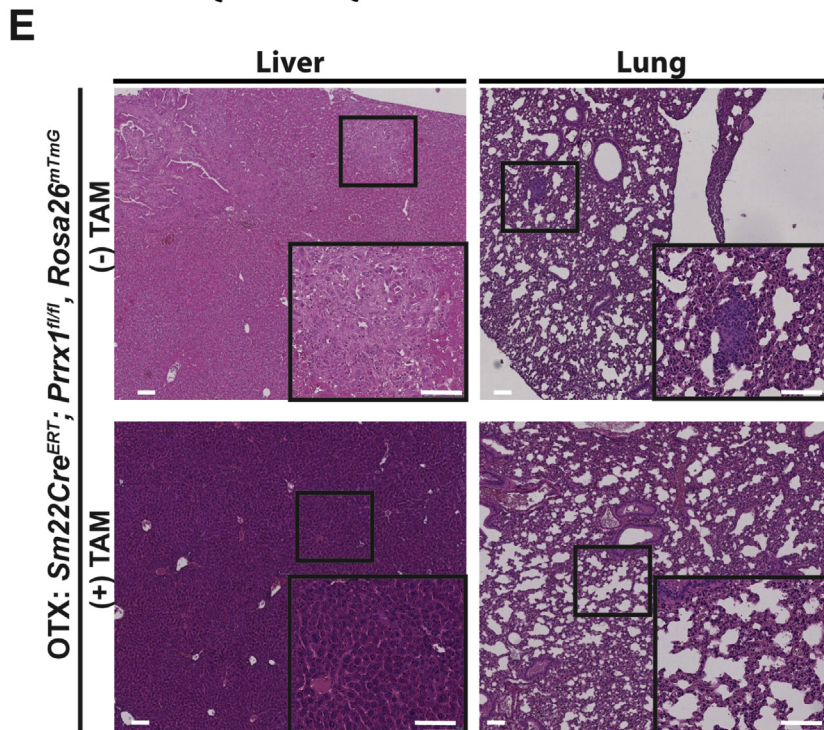
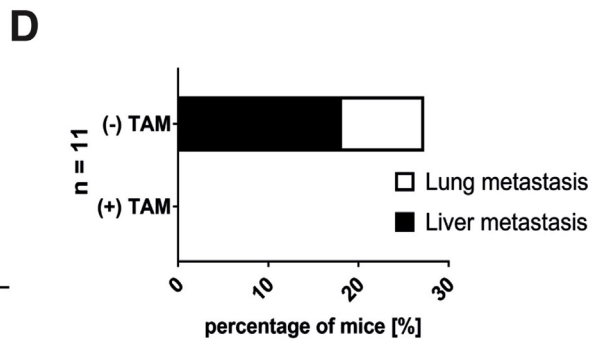
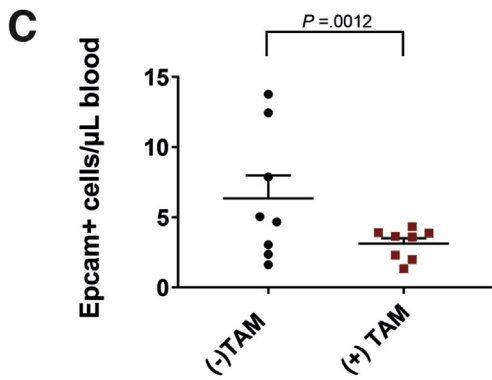
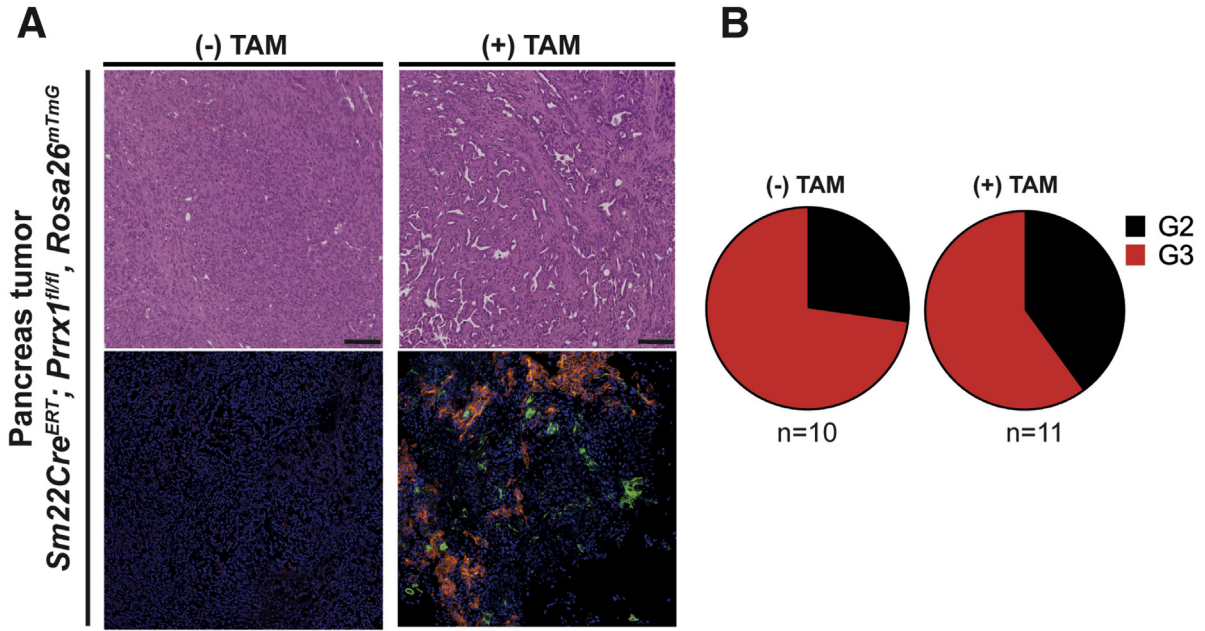
As shown earlier, stromal *Prrx1* correlates with distinct pancreatic subtypes and tumor differentiation (Figures 1G and H and 4A and B). To explore the influence of FB-

secreted factors on tumor cell differentiation, coculture experiments (with permeable Transwell [Corning, NY] inserts to maintain separation of the 2 cell types) were performed in vitro (Figure 6A). Coculturing tumor cells with FBs per se leads to significantly higher expression of EMT and ECM markers in tumor cells compared with tumor cells cultured alone, confirming that FBs can induce tumor cells to undergo EMT (Figure 7B). Remarkably, coculturing FBs lacking *Prrx1* overcomes this effect and leads to reduced expression of EMT markers, such as *Hgf*, *Twist*, *Zeb1*, *Slug*, and *Etv1*, as well as reduced levels of ECM markers, for example, periostin and tenascin-C (Figure 6B).

Next, we analyzed the phenotype of the tumor cells in a 3D collagen assay (organoid culture), as illustrated in Figure 6C. FBs were grown on the bottom of plastic dishes, and tumor cells were placed on top of the FBs, embedded into a layer of collagen. Immunofluorescence staining showed that cancer cells cocultured with wild-type FBs exhibit a reduced capacity to form a spheroid structure and express a high α -SMA level, indicating that these tumor cells undergo EMT (Figure 6D). By contrast, tumor cells cocultured with *Prrx1*^{f/f} FBs retain their epithelial integrity and form organized spheroidal structures lacking α -SMA expression (Figure 6D). Next, we determined anchorage-independent growth of PDAC cells while culturing them with the supernatant generated from *Prrx1*-proficient and *Prrx1*-knockout FBs. We observed a significant decrease of colony formation in soft agarose of PDAC cells treated with *Prrx1*-knockout FB-conditioned media compared to controls, indicating reduced outgrowth (Supplementary Figure 12B). Hence, *Prrx1* in CAFs seem to promote seeding (Figure 4C) as well as outgrowth of pancreatic tumor cells.

TGF- β is an EMT inducer in several different tissue types,⁴⁶ and one major source of TGF- β in addition to the tumor cells is CAFs.^{47,48} To evaluate whether *Prrx1* alters TGF- β secretion in CAFs and thereby affects the epithelial differentiation of tumor cells, TGF- β secretion was assessed by enzyme-linked immunosorbent assay (ELISA). There was no significant difference in TGF- β secretion between *Prrx1*-proficient and *Prrx1*-knockout FBs, indicating that TGF- β does not contribute to the observed phenotype (Supplementary Figure 12C). Also, CAF-derived HGF has been found to promote EMT in tumor cells by activation of the MET pathway.⁴⁹ As we have shown in tumor cells previously, *Prrx1b* regulates HGF-dependent MET activation and plays an important role in stimulating EMT, resulting in increased invasion and metastasis.²³ To explore this avenue in CAFs, we analyzed the HGF level in the supernatant of single- and coculture in vitro assays. As determined by HGF ELISA, tumor cells secrete only small amounts of HGF (Figure 6E). In contrast, conditioned

Figure 3. Loss of *Prrx1* in FBs leads to dramatic changes of the TME in the orthotopic *Sm22-Cre^{ERT};Prrx1^{f/f}* model. (A) Representative image of Elastic van Gieson staining, fibronectin staining, and picosirius red staining; scale bar, 100 μ m. (B) Representative IF staining of the merge picture (right corner) and IF staining for SPARC, collagen I, and α -SMA; scale bar, 50 μ m. (C) Semiquantitative image processing was used to quantify SPARC staining, unpaired Student *t* test; ***P* = .0016. (D) Semiquantitative image processing was used to quantify collagen I staining, unpaired Student *t* test; ***P* = .0047. (E) Semiquantitative image processing was used to quantify α -SMA staining, unpaired Student *t* test; **P* = .03. (F) Representative IHC staining for macrophages (F4/80), B cells (CD45R), T cells (CD3), T helper cells (CD4), cytotoxic T cells (CD8), and dendritic cells (MHC II) in PDAC tissues; scale bar, 100 μ m. Data were analyzed by using an unpaired Student *t* test. FOV, field of view; OTX, orthotopic transplantation model.



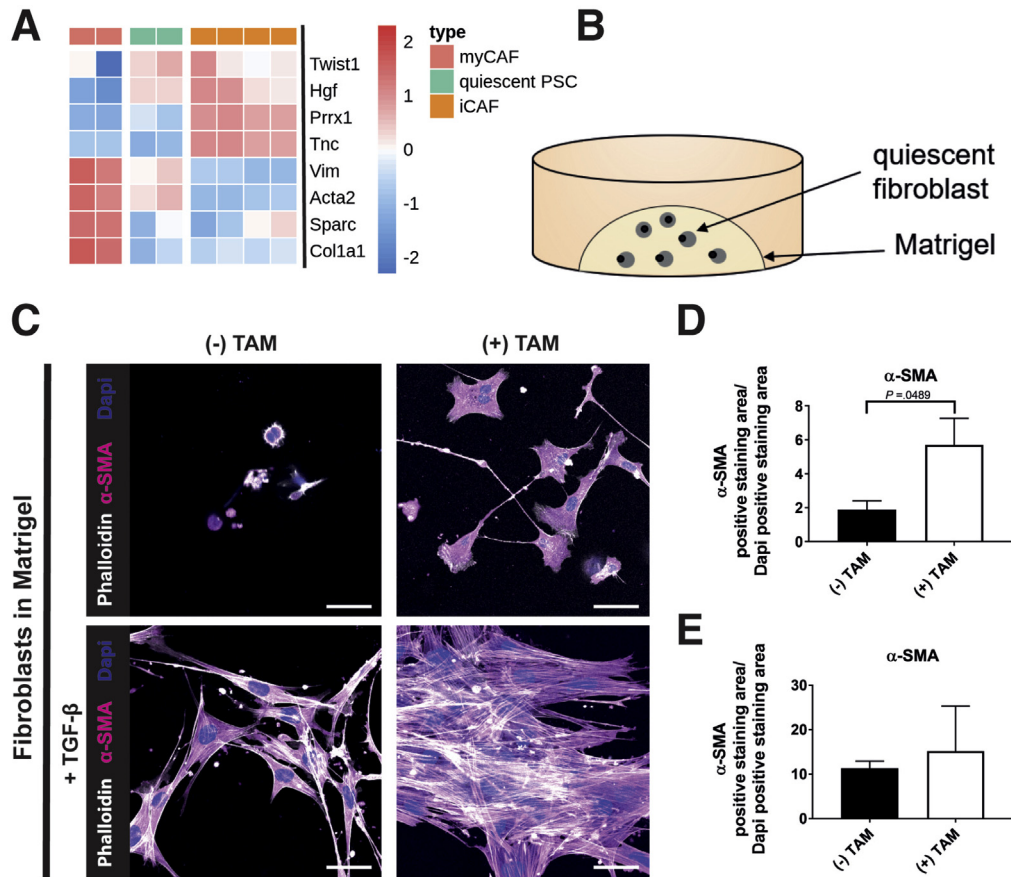


Figure 5. Reduced plasticity in *Prrx1*-deficient FBs. (A) RNA-seq data of quiescent PSCs, iCAFs, and myCAFs from Öhlund et al.²⁰ Heat map shows differentially expressed genes among the 3 cell states. (B) Illustration of the experimental design. (C) PSCs cultured in Matrigel; 3 PSC cell lines were used. Representative IF staining for phalloidin, α -SMA, and DAPI; scale bar, 50 μ m; lower row: +TGF- β . (D, E) Semi-quantitative image processing was used to quantify α -SMA staining normalized to DAPI staining; unpaired Student *t* test, **P* = .0468. DAPI, 4',6-diamidino-2-phenylindole.

media of cocultured CAFs and tumor cells show high abundance of HGF. Importantly, HGF secretion is significantly reduced in coculture conditioned media of *Prrx1*-deficient FBs (Figure 6E). To validate our findings in vivo, we performed HGF immunohistochemistry staining of pancreatic tumors and analyzed HGF protein levels in the serum of mice from our orthotopic model. Mice with *Prrx1*-deficient FBs exhibited reduced HGF expression by IHC as well as decreased HGF protein abundance in serum, underscoring our in vitro findings (Figure 6F and G). To further illustrate the significance of the *Prrx1*-Hgf axis in CAFs, we performed gemcitabine treatment in coculture in a Transwell assay (Figure 6H). We measured a higher sensitivity to gemcitabine when tumor cells were cocultured with *Prrx1*-deficient FBs compared to control FBs (Figure 6H). Importantly, this observation was likely not due to altered drug uptake or drug metabolism (Supplementary Figure 12D).

The addition of recombinant HGF to cocultures overrode the effect of *Prrx1* ablation in CAFs and restored the more

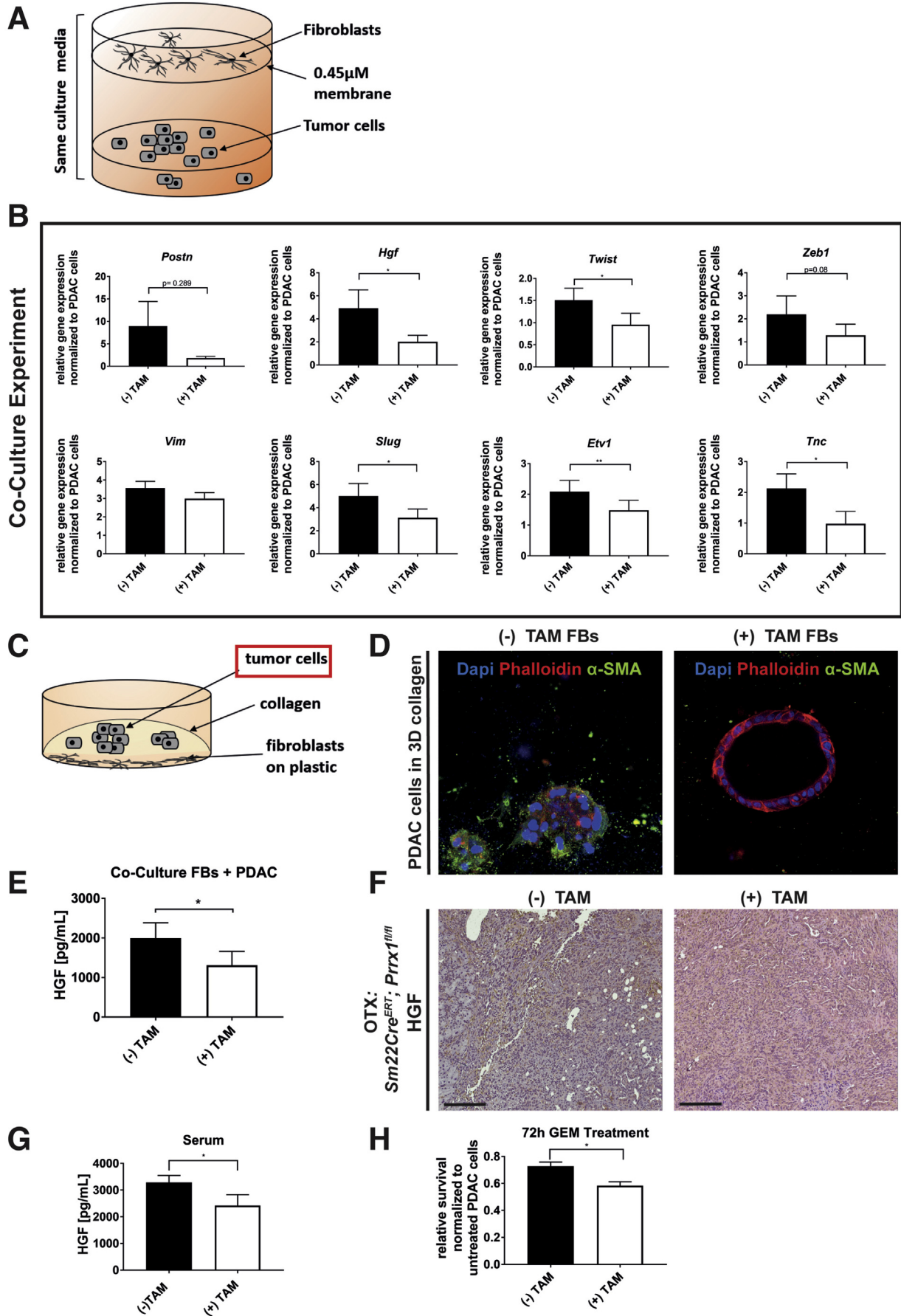
mesenchymal phenotype of the tumor cells indicated by upregulation of EMT markers *Postn*, *Twist*, *Zeb1*, *Vim*, *Slug*, *Etv1*, and *Tnc* (Figure 7A). Additionally, gemcitabine treatment of a coculture system with recombinant HGF showed higher chemoresistance, restoring the effect of *Prrx1* ablation in CAFs (Figure 7B).

Together, these data provide strong evidence that *Prrx1* in CAFs alters tumor differentiation and gemcitabine response through paracrine HGF signaling.

Conclusion

CAF s constitute a diverse cell population consisting of several subtypes. For example, quiescent PSCs can give rise to iCAFs, myCAFs, and antigen-presenting CAFs, which are interconvertible states leading to intratumoral CAF heterogeneity.^{20,29} This complexity might help explain contradictory results in attempts to target the stroma in the past.^{12,14,15,50,51} In search of a molecular driver of

Figure 4. Changes in tumor differentiation, dissemination, and metastasis upon stromal *Prrx1* depletion. (A) Upper row: H&E staining of PDAC in the control (-) TAM- and *Prrx1*^{fl/fl} (+) TAM-treated mice; scale bar, 100 μ m. Lower row: IF of cryosection with endogenous tdTomato and eGFP signal; DAPI staining; scale bar, 100 μ m. (B) Tumor grading at the 2-week timepoint. (C) FACS analysis of EpCAM⁺ cells isolated from the whole-body blood of mice; n = 8 per group; unpaired Student *t* test; *P* = .0012. (D) Quantification of liver and lung metastasis of n = 11 per group. (E) H&E staining of liver and lung tissue at the tw2o-week timepoint. Upper row: control mouse with lung and liver metastasis. Lower row: (+) TAM, normal lung and liver tissue, no metastasis. DAPI, 4',6-diamidino-2-phenylindole; FACS, fluorescence-activated cell sorting.



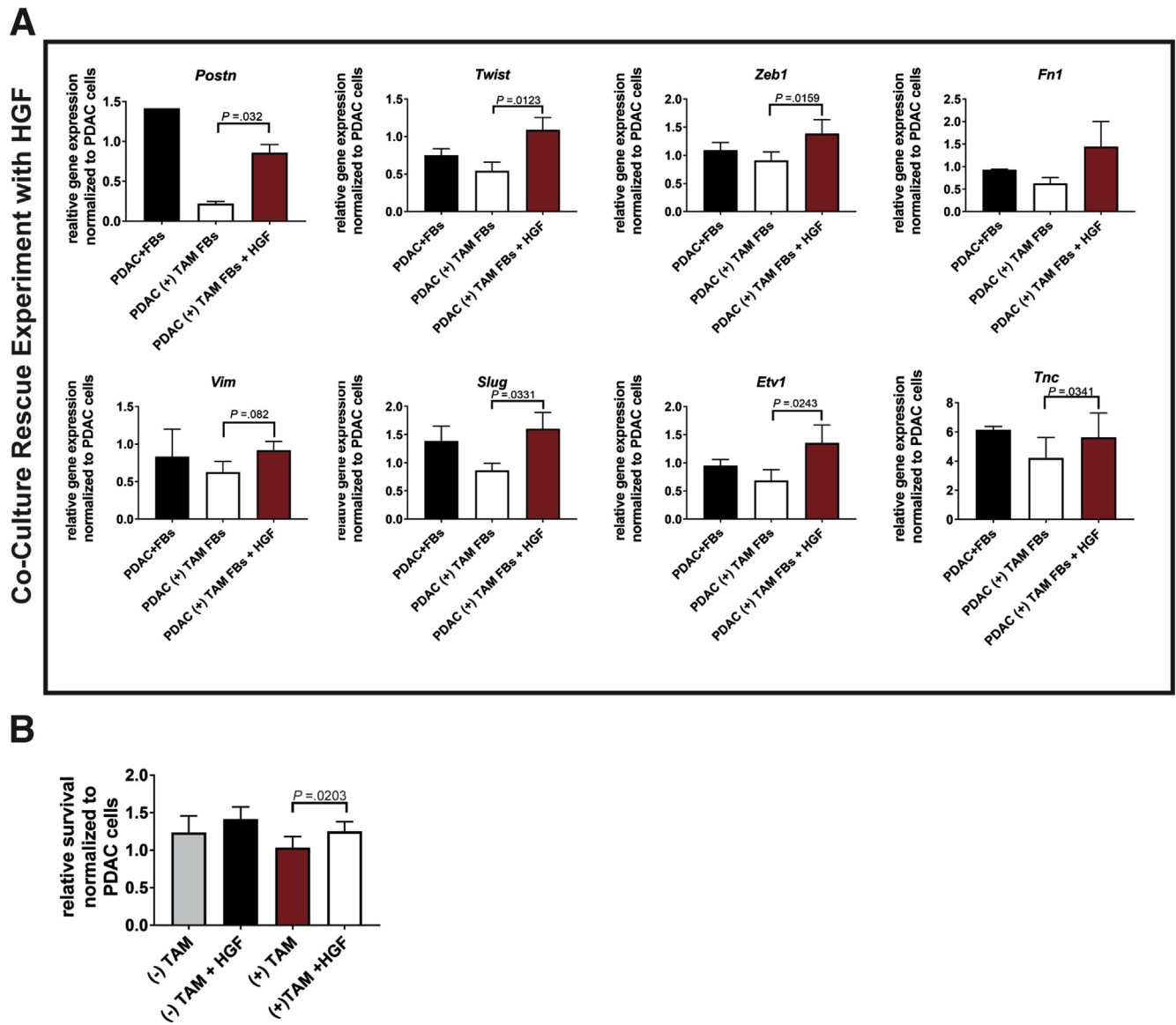


Figure 7. Recombinant HGF can rescue the effect of *Prrx1* knockdown. (A) qPCR analysis of EMT markers expressed in tumor cells cocultured with FBs \pm HGF. Paired Student *t* test; $n = 6$ (3 independent cell lines). (B) MTT assay of tumor cells cocultured with FBs \pm HGF after 72 hours of gemcitabine treatment (600 nmol/L gemcitabine); unpaired Student *t* test (3 independent cell lines).

intratumoral CAF plasticity, we focused on the transcription factor *Prrx1* because we have previously identified *Prrx1* regulating processes involving highly dynamic cell-fate decisions, including pancreatic organogenesis, regeneration, and carcinogenesis.^{22,23} Yeo et al²⁶ and Sangrador et al⁵²

influences carcinogenesis. We hypothesized that *Prrx1*-driven CAF plasticity shapes the tumor-stroma crosstalk in PDAC. Indeed, cross-compartment analysis of 2 independent data sets from Moffitt et al³¹ and Nicolle et al²⁸ shows that high-stromal *Prrx1* expression correlates with the squamous subtype of PDAC.

Figure 6. *Prrx1*-proficient FBs induce EMT in tumor cells via HGF signaling. (A) Illustration of the Transwell coculture experiment. (B) qPCR analysis of EMT markers expressed in tumor cells cocultured with FBs; paired Student *t* test (3 independent cell lines). (C) Illustration of the 3D coculture experiment. (D) 3D coculture experiment with representative IF staining of tumor cells for α -SMA, phalloidin, and DAPI; scale bar, 50 μ m. (E) HGF ELISA of the supernatant from tumor cells cocultured with FBs in a Transwell; unpaired Student *t* test (3 independent cell lines). (F) Representative image of HGF staining (IHC). $n = 3$ per group of *Sm22-Cre^{ERT};Prrx1^{fl/fl}* mice after 14 days; scale bar, 200 μ m. (G) HGF ELISA of serum from *Sm22-Cre^{ERT};Prrx1^{fl/fl}* mice 14 days after tumor cell implantation. $n = 4$ per group; unpaired Student *t* test; $*P < .05$. (H) MTT assay of tumor cells cocultured with FBs after 72 hours of gemcitabine treatment (600 nmol/L gemcitabine); unpaired Student *t* test (3 independent cell lines).

Our *in vivo* data further confirm the important role of Prrx1 in PDAC development. Specifically, we show that Prrx1 in CAFs restrains stromal expansion, promotes invasion as well as dissemination of tumor cells into the blood circulation, and fosters metastasis. We prove that *Prrx1*-deficient CAFs support stromal expansion by ECM protein secretion, restrain tumor dedifferentiation, and disrupt tumor dissemination. Additionally, we observed an increase in lymphocyte infiltration, especially in B cells, T-helper, and cytotoxic T cells. These results are consistent with the findings of Özdemir et al.¹⁵ and Rhim et al.,¹⁴ who showed that the TME restrains rather than supports tumor growth.^{14,15} Importantly, depletion of α -SMA⁺ FBs led to altered immune infiltration, for example, inhibition of T regulatory cells.¹⁵ Immune-modulatory properties of CAFs are present across diverse cancer types, for example, promoting macrophage recruitment, immune suppression, and tumor growth through the secretion of cytokines and chemokines such as IL6, IL1 β , and CXCL1.^{21,53,54} Interestingly, *Prrx1*-proficient FBs promote an immune-evasive phenotype, as characterized by reduced levels of cytotoxic and helper T cells, which might explain a more aggressive PDAC phenotype.

Notably, the 3D-Matrigel assay and gene expression profiling showed that the loss of *Prrx1* in FBs leads to reduced plasticity; these cells remain in their activated state and cannot revert back to their quiescent state.²⁰ On a separate note, isoform-specific rescue of Prrx1 expression indicates that *Prrx1b* is able to suppress α -SMA expression, whereas FBs with transgenic expression of *Prrx1a* remain in their highly activated state. These data indicate that the switch from Prrx1a to Prrx1b expression or vice versa also plays an important role to promote FB plasticity, as we have already shown for Prrx1 isoforms in tumor cells.²³ In summary, Prrx1 appears to be a plasticity driver in FBs that directly controls their myofibroblastic phenotype and sustains their protumorigenic properties.

Apart from cancer, mesodermal Prrx1 is highly expressed during embryonic development as well as other nonhomeostatic conditions. For example, a transcriptional program including *Prrx1*, *Msx1*, and *Pdgfra* was identified in mouse digit tip regeneration at single-cell resolution.⁵⁵ In the context of idiopathic pulmonary fibrosis, it was shown that increased matrix stiffness suppresses Prrx1 expression, indicating a potential feedback loop in which Prrx1 regulates biophysical properties of the ECM which, in turn, modulates Prrx1 expression.⁵⁶

We have reported that tumor cell-derived HGF is a transcriptional target of PRRX1B.²³ These findings led to the initiation of a clinical trial testing the combination of the anti-HGF antibody, ficlatuzumab (AV-299), in combination with gemcitabine and nab-paclitaxel in patients with advanced PDAC (NCT03316599). Strikingly, now we have discovered the importance of the Prrx1-Hgf axis in CAFs, including the impact on tumor differentiation and response to gemcitabine treatment, possibly adding to the rationale for this clinical trial.

In vivo and *in vitro* data show that activated FBs can foster PDAC progression through paracrine signaling.⁸ CAFs

are a rich source of active soluble factors that support the growth, proliferation, migration, and drug resistance of tumor cells in a non-cell-autonomous manner.^{57,58} Consistent with this notion, our work proves that culture-activated CAFs exert paracrine tumor-supporting effects on PDAC cells. Two recent publications have described iCAF and myCAF as interconvertible cell states rather than endpoints in differentiation.^{20,21} We suggest that targeting Prrx1 in FBs is able to convert potential tumor-promoting into tumor-restraining CAFs. The efficacy of this strategy was illustrated previously by transcriptional reprogramming of activated FBs into quiescent PSCs.¹¹ In contrast to this study, we propose reducing CAF plasticity by forcing myCAF differentiation. Taken together, our results indicate that targeting the plasticity of FBs has a significant impact on tumor biology. These data highlight the possibilities of new treatment strategies through the conversion of tumor-promoting CAFs into tumor-restraining CAFs.

Supplementary Material

Note: To access the supplementary material accompanying this article, visit the online version of *Gastroenterology* at www.gastrojournal.org, and at <https://doi.org/10.1053/j.gastro.2020.09.010>.

References

1. Öhlund D, Elyada E, Tuveson D. Fibroblast heterogeneity in the cancer wound. *J Exp Med* 2014;211:1503–1523.
2. Kalluri R, Zeisberg M. Fibroblasts in cancer. *Nat Rev Cancer* 2006;6:392–401.
3. Erkan M, Michalski CW, Rieder S, et al. The activated stroma index is a novel and independent prognostic marker in pancreatic ductal adenocarcinoma. *Clin Gastroenterol Hepatol* 2008;6:1155–1161.
4. Awaji M, Singh R. Cancer-associated fibroblasts' functional heterogeneity in pancreatic ductal adenocarcinoma. *Cancers (Basel)* 2019;11(3):290.
5. Strutz F, Okada H, Lo CW, et al. Identification and characterization of a fibroblast marker: FSP1. *J Cell Biol* 1995;130:393–405.
6. Kalluri R. The biology and function of fibroblasts in cancer. *Nat Rev Cancer* 2016;16:582–598.
7. LeBleu VS, Kalluri R. A peek into cancer-associated fibroblasts: origins, functions and translational impact. *Dis Model Mech* 2018;11(4):dmm029447.
8. Vonlaufen A, Joshi S, Qu C, et al. Pancreatic stellate cells: partners in crime with pancreatic cancer cells. *Cancer Res* 2008;68:2085–2093.
9. Feig C, Gopinathan A, Neesse A, et al. The pancreas cancer microenvironment. *Clin Cancer Res* 2012;18:4266–4276.
10. Kikuta K, Masamune A, Watanabe T, et al. Pancreatic stellate cells promote epithelial-mesenchymal transition in pancreatic cancer cells. *Biochem Biophys Res Commun* 2010;403:380–384.
11. Sherman MH, Yu RT, Engle DD, et al. Vitamin D receptor-mediated stromal reprogramming suppresses

- pancreatitis and enhances pancreatic cancer therapy. *Cell* 2014;159:80–93.
12. Olive KP, Jacobetz MA, Davidson CJ, et al. Inhibition of Hedgehog signaling enhances delivery of chemotherapy in a mouse model of pancreatic cancer. *Science* 2009;324(5933):1457–1461.
 13. Infinity Pharmaceuticals. A study evaluating IPI-926 in combination with gemcitabine in patients with metastatic pancreatic cancer. *ClinicalTrials.gov*. <https://clinicaltrials.gov/ct2/show/NCT01130142>. Published May 25, 2010. Updated March 6, 2017. Accessed November 16, 2020.
 14. Rhim AD, Oberstein PE, Thomas DH, et al. Stromal elements act to restrain, rather than support, pancreatic ductal adenocarcinoma. *Cancer Cell* 2014;25:735–747.
 15. Özdemir BC, Pentcheva-Hoang T, Carstens JL, et al. Depletion of carcinoma-associated fibroblasts and fibrosis induces immunosuppression and accelerates pancreas cancer with reduced survival. *Cancer Cell* 2014;25:719–734.
 16. Provenzano PP, Cuevas C, Chang AE, et al. Enzymatic targeting of the stroma ablates physical barriers to treatment of pancreatic ductal adenocarcinoma. *Cancer Cell* 2012;21:418–429.
 17. Jacobetz MA, Chan DS, Neesse A, et al. Hyaluronan impairs vascular function and drug delivery in a mouse model of pancreatic cancer. *Gut* 2013;62:112–120.
 18. Huang Y, Goel S, Duda DG, et al. Vascular normalization as an emerging strategy to enhance cancer immunotherapy. *Cancer Res* 2013;73:2943–2948.
 19. Kildani A. Halozyme announces HALO-301 phase 3 study fails to meet primary endpoint. Halozyme. <https://www.halozyme.com/investors/news-releases/news-release-details/2019/Halozyme-Announces-HALO-301-Phase-3-Study-Fails-To-Meet-Primary-Endpoint/default.aspx>. Accessed November 16, 2020.
 20. Öhlund D, Handly-Santana A, Biffi G, et al. Distinct populations of inflammatory fibroblasts and myofibroblasts in pancreatic cancer. *J Exp Med* 2017;214:579–596.
 21. Biffi G, Oni TE, Spielman B, et al. IL-1-induced JAK/STAT signaling is antagonized by TGF β to shape CAF heterogeneity in pancreatic ductal adenocarcinoma. *Cancer Discov* 2019;9:282–301.
 22. Reichert M, Takano S, von Burstin J, et al. The Prrx1 homeodomain transcription factor plays a central role in pancreatic regeneration and carcinogenesis. *Genes Dev* 2013;27:288–300.
 23. Takano S, Reichert M, Bakir B, et al. Prrx1 isoform switching regulates pancreatic cancer invasion and metastatic colonization. *Genes Dev* 2016;30:233–247.
 24. Reichert M, Takano S, Heeg S, et al. Isolation, culture and genetic manipulation of mouse pancreatic ductal cells. *Nat Protoc* 2013;8:1354–1365.
 25. Heeg S, Das KK, Reichert M, et al. ETS-transcription factor ETV1 regulates stromal expansion and metastasis in pancreatic cancer. *Gastroenterology* 2016;151:540–553.
 26. Yeo S-Y, Lee K-W, Shin D, et al. A positive feedback loop bi-stably activates fibroblasts. *Nat Commun* 2018;9:3016.
 27. Tomaru Y, Hasegawa R, Suzuki T, et al. A transient disruption of fibroblastic transcriptional regulatory network facilitates trans-differentiation. *Nucleic Acids Res* 2014;42:8905–8913.
 28. Nicolle R, Blum Y, Marisa L, et al. Pancreatic adenocarcinoma therapeutic targets revealed by tumor-stroma cross-talk analyses in patient-derived xenografts. *Cell Rep* 2017;21:2458–2470.
 29. Elyada E, Bolisetty M, Laise P, et al. Cross-species single-cell analysis of pancreatic ductal adenocarcinoma reveals antigen-presenting cancer-associated fibroblasts. *Cancer Discov* 2019;9:1102–1123.
 30. Peng J, Sun B-F, Chen C-Y, et al. Single-cell RNA-seq highlights intra-tumoral heterogeneity and malignant progression in pancreatic ductal adenocarcinoma. *Cell Res* 2019;29:725–738.
 31. Moffitt RA, Marayati R, Flate EL, et al. Virtual microdissection identifies distinct tumor- and stroma-specific subtypes of pancreatic ductal adenocarcinoma. *Nat Genet* 2015;47:1168–1178.
 32. Collisson EA, Sadanandam A, Olson P, et al. Subtypes of pancreatic ductal adenocarcinoma and their differing responses to therapy. *Nat Med* 2011;17:500–503.
 33. Bailey P, Chang DK, Nones K, et al. Genomic analyses identify molecular subtypes of pancreatic cancer. *Nature* 2016;531:47–52.
 34. The Cancer Genome Atlas Research Network. Integrated genomic characterization of pancreatic ductal adenocarcinoma. *Cancer Cell* 2017;32:185–203.
 35. Martin JF, Bradley A, Olson EN. The paired-like homeobox gene MHOX is required for early events of skeletogenesis in multiple lineages. *Genes Dev* 1995;9:1237–1249.
 36. Martin JF, Olson EN. Identification of a prx1 limb enhancer. *Genesis* 2000;26:225–229.
 37. Kühbandner S, Brummer S, Metzger D, et al. Temporally controlled somatic mutagenesis in smooth muscle. *Genesis* 2000;28:15–22.
 38. Muzumdar MD, Tasic B, Miyamichi K, et al. A global double-fluorescent Cre reporter mouse. *Genesis* 2007;45:593–605.
 39. Pure E, Hingorani SR. Mesenchymal cell plasticity and perfidy in epithelial malignancy. *Trends Cancer* 2018;4:273–277.
 40. Marchand B, Pitarresi JR, Reichert M, et al. PRRX1 isoforms cooperate with FOXM1 to regulate the DNA damage response in pancreatic cancer cells. *Oncogene* 2019;38:4325–4339.
 41. Schwarz RI. Collagen I and the fibroblast: high protein expression requires a new paradigm of post-transcriptional, feedback regulation. *Biochem Biophys Rep* 2015;3:38–44.
 42. Schönhuber N, Seidler B, Schuck K, et al. A next-generation dual-recombinase system for time- and host-specific targeting of pancreatic cancer. *Nat Med* 2014;20:1340–1347.
 43. McKean DM, Sisbarro L, Ilic D, et al. FAK induces expression of Prx1 to promote tenascin-C-dependent fibroblast migration. *J Cell Biol* 2003;161:393–402.

44. Ocaña OH, Córcoles R, Fabra A, et al. Metastatic colonization requires the repression of the epithelial-mesenchymal transition inducer Prrx1. *Cancer Cell* 2012;22:709–724.
45. Jesnowski R, Fürst D, Ringel J, et al. Immortalization of pancreatic stellate cells as an in vitro model of pancreatic fibrosis: deactivation is induced by matrigel and N-acetylcysteine. *Lab Invest* 2005;85:1276–1291.
46. Dongre A, Weinberg RA. New insights into the mechanisms of epithelial–mesenchymal transition and implications for cancer. *Nat Rev Mol Cell Biol* 2019;20:69–84.
47. Erdogan B, Webb DJ. Cancer-associated fibroblasts modulate growth factor signaling and extracellular matrix remodeling to regulate tumor metastasis. *Biochem Soc Trans* 2017;45:229–236.
48. Yu Y, Xiao C-H, Tan L-D, et al. Cancer-associated fibroblasts induce epithelial-mesenchymal transition of breast cancer cells through paracrine TGF- β signalling. *Br J Cancer* 2014;110:724–732.
49. Ding X, Ji J, Jiang J, et al. HGF-mediated crosstalk between cancer-associated fibroblasts and MET-unamplified gastric cancer cells activates coordinated tumorigenesis and metastasis. *Cell Death Dis* 2018; 9(9):867.
50. Lee JJ, Perera RM, Wang H, et al. Stromal response to Hedgehog signaling restrains pancreatic cancer progression. *Proc Natl Acad Sci U S A* 2014;111(30):E3091–E3100.
51. Bailey JM, Swanson BJ, Hamada T, et al. Sonic hedgehog promotes desmoplasia in pancreatic cancer. *Clin Cancer Res* 2008;14:5995–6004.
52. Sangrador I, Molero X, Campbell F, et al. Zeb1 in stromal myofibroblasts promotes *Kras*-driven development of pancreatic cancer. *Cancer Res* 2018;78:2624–2637.
53. Sun Q, Zhang B, Hu Q, et al. The impact of cancer-associated fibroblasts on major hallmarks of pancreatic cancer. *Theranostics* 2018;8:5072–5087.
54. Kuen J, Darowski D, Kluge T, Majety M. Pancreatic cancer cell/fibroblast co-culture induces M2 like macrophages that influence therapeutic response in a 3D model. *PLoS One* 2017;12(7):e0182039.
55. Johnson GL, Masias EJ, Lehoczy JA. Cellular heterogeneity and lineage restriction during mouse digit tip regeneration at single-cell resolution. *Dev Cell* 2020; 52:525–540.
56. Froidure A, Marchal-Duval E, Ghanem M, et al. Mesenchyme associated transcription factor PRRX1: a key regulator of IPF fibroblast. *Eur Respir J* 2016; 48:OA506.
57. Apte MV, Wilson JS, Lugea A, et al. A starring role for stellate cells in the pancreatic cancer microenvironment. *Gastroenterology* 2013;144:1210–1219.
58. Hwang RF, Moore T, Arumugam T, et al. Cancer-associated stromal fibroblasts promote pancreatic tumor progression. *Cancer Res* 2008;68:918–926.

Received December 11, 2019. Accepted September 6, 2020.

Correspondence

Address correspondence to: Maximilian Reichert, MD, Technical University of Munich, Klinik and Poliklinik für Innere Medizin II, Trogerstr. 32, 81371, München Germany. e-mail: maximilian.reichert@tum.de; fax: 49 89 4140 2469.

Conflicts of interest

The authors disclose no conflicts.

Funding

Karin Feldmann and Maximilian Reichert are supported by the German Cancer Aid Foundation (Max Eder Program, Deutsche Krebshilfe 111273, Maximilian Reichert) and the German Research Foundation (RE 3723/4-1 and SFB1321/Project ID 329628492). Maximilian Reichert, Katja Pescke, Kathleen Schuck, Aristeidis Papargyriou, Thomas Engleitner, Rupert Öllinger, Wilko Weichert, Roland M. Schmid, Günter Schneider, Roland Rad, and Dieter Saur are supported by the German Research Foundation (Deutsche Forschungsgemeinschaft, SFB1321/project ID 329628492 Modeling and Targeting Pancreatic Cancer). Günter Schneider is supported by German Research Foundation (SCHN 959/3-1) and the DTK Joint funding program. Kathleen Schuck and Wilko Weichert are supported by the German Research Foundation (Deutsche Forschungsgemeinschaft, SFB824).

Supplementary Experimental Procedures

Cell Line, Cell Culture, and In Vitro Assays

Tumor cells and FBs were isolated as previously described.¹ Tumor cells were cultivated in Dulbecco's modified Eagle medium (DMEM) (Gibco, Waltham, MA; no. 41966052), 10% fetal bovine serum (FBS) (Gibco no. 10270106), and 1% penicillin/streptomycin (P/S) (Gibco no. 1741838). FBs were resuspended in PSC medium (20% FBS; 1% P/S in 50% DMEM-F12 [Gibco no. 31330095] and DMEM low glucose [Gibco no. 11885084]), then cultured on plastic dishes. The protocol for isolating PSCs was based on a previous method,² with some modifications. Detailed information is provided in the "Primary Pancreatic Stellate Cells" section. In vitro recombination was performed with 500 nmol/L 4-OTH TAM (Sigma, St Louis, MO; no. H7904) 3 times per week. The migration assay was performed as described by Demir et al³ and the adhesion assay as described in Böttcher et al⁴ for collagen type I. To activate the transcription of Prrx1a and Prrx1b (Tet-on system) of the Prrx1a FBs and Prrx1b FBs, the FBs were treated with 1 μ g/mL doxycyclin. We thank Dr Kaori Ihida-Stansbury (University of Pennsylvania) for the PRRX1 wild-type and knockout mouse embryonic FBs and Stefanie Bärthel for the SB1560 cell line. For all in vitro experiments, 3–5 different primary FB cell lines, including PSC cell lines, were used. All experiments were performed in triplicate. Error bars represent the standard error of the mean.

Primary Pancreatic Stellate Cells

Before starting the isolation, Gey's balanced salt solution (GBSS) for 500 mL was prepared as follows: 0.105 g MgCl₂ 6H₂O, 0.0171 g MgSO₄ anhydrous, 0.185 g KCl, 0.15 g KH₂PO₄ anhydrous, 0.0598 g Na₂HPO₄ anhydrous, 1.135 g NaHCO₃, 0.5 g glucose, and 0.1126 g CaCl₂. Once the pancreas had been isolated, it was infiltrated with GBSS/0.3% bovine serum albumin (BSA) (A2058-1G; Sigma)/1 mg/mL Collagenase P solution (Roche, Indianapolis, IN; no. 11 213 857 001) and then cut into pieces. The resulting suspension was incubated at 37°C for approximately 15 minutes. After centrifugation (1000g, 5 minutes), the pellet was resuspended in GBSS/0.3% BSA/0.5% trypsin solution and incubated for 5 minutes at 37°C. The digested pancreas suspension was filtered through a 100- μ m nylon mesh and centrifuged (1000g, 5 minutes). The pellet was resuspended in 4.75 mL GBSS/0.3% BSA and 4 mL 28.7% Nycodenz (Sigma, no. D2158-100g) in Gey's solution without NaCl was added. A layer of 3 mL GBSS/0.3% BSA was added to the top of the solution. The solution was centrifuged at 1400g for 20 minutes at 4°C, without a break, to form a gradient. The white layer above the interface was collected and resuspended in GBSS/0.3% BSA solution. After further centrifugation (1000g, 5 minutes), the cells were resuspended in PSC medium (20% FBS; 1% P/S in 50% DMEM-F12 [Gibco no. 31330095] and DMEM low glucose [Gibco no. 11885084]).

Lentiviral Production and Transduction

Lentiviruses were produced in HEK293T cells. In brief, HEK293T cells were transfected in a 100-mm dish using Lipofectamine 2000 (Thermo Fisher Scientific, Waltham, MA; no. 11668019) with 10 μ g of pTRIPz-Prrx1a and pTRIPz-Prrx1b plasmid (previously published in Reichert et al⁵) and 6.5 μ g of the lentiviral packaging plasmids psPAX2 and 3.5 μ g pMD2 VSVG. After 48 hours, the supernatant was harvested and filtered through a 0.45- μ m filter. The embryonic Prrx1-knockout FBs were infected with viral suspension containing 4 μ g/mL of polybrene (Millipore, Burlington, MA; no. TR-1003-G) and centrifuged for 45 minutes at 1800 revolutions/minute at room temperature. This step was repeated, and afterward, the cells were grown overnight by 37°C by 5% CO₂. After the media change, the infected cells were selected with 2 μ g/mL puromycin (Thermo Fisher Scientific, no. A1113803) for generation of stable Prrx1a-FB and Prrx1b-FB.

Transwell Coculture Experiments

For cocultures, PDAC cells were seeded in the bottom layer of a Transwell tray, and FBs (3 different FB cell lines were used) were seeded in an equal number on top of the Transwell membrane (0.45- μ m pore size) (Corning, Corning, NY). The cells were cultured in 50% DMEM F12 plus 50% DMEM low glucose, 2% FBS, and 1% P/S for 3 days. For drug testing, gemcitabine (600 nmol/L) was added to the cells 12 hours after seeding. The plates were measured for MTT (Sigma, no. M5655) 72 hours after adding the drug.

Three-Dimensional Organoid Culture and Immunofluorescence

For IF staining, the cells were fixed with 4% paraffin formaldehyde solution (Sigma no. 158127) for 30 minutes at room temperature and then permeabilized with a permeabilization solution consisting of 0.35 g fish-skin gelatin (Sigma, no. G7765) and 250 μ L Triton X-100 diluted in 50 mL phosphate-buffered saline (PBS) with Ca²⁺ and Mg²⁺ (PBS+) (Invitrogen, San Diego, CA; no. 14040) for an additional 30 minutes at room temperature while rocking. Primary antibodies were diluted in permeabilization solution, and the cells with the diluted antibody were incubated overnight at 4°C. After 3 washing steps, the secondary antibodies were diluted in permeabilization solution and incubated either overnight at 4°C or for 3 hours at room temperature. Subsequent washing steps with permeabilization solution and PBS followed before the cells were mounted (VECTASHIELD, Vector Laboratories, Burlingame, CA; no. H-1200) with a coverslip.

Anchorage-Independent Growth

The (-) TAM and (+) TAM FBs were seeded in equal numbers for 3 to 4 days in T75 flasks with 2% FBS. The supernatant was harvested and filtered through a 0.45- μ m membrane. The filtered supernatant was mixed with 1:1 with 1% agarose (UltraPure LMP Agarose; Invitrogen, no. 16520-

050). Six-well plates were coated with 1 mL of the mixtures and solidified under the hood. Afterward, 10,000 tumor cells/well were added to a mixture of 1% agarose and the FB supernatant and 2 mL/well seeded on top of the precoated well. The plates were solidified under the hood and 500 μ L FB supernatant was added before placing them into the incubator (37°C, 5% CO₂). Twice a week, 200 μ L supernatant was added to the plate to prevent dehydration. After 2 weeks, colonies were stained by adding 500 μ L Thiazolyl Blue Tetrazolium Bromide solution (0.5 mg/mL) (Sigma, no. M5655) to each well. After 3 hours of incubation (37°C, 5% CO₂), images were taken, and the colonies were counted.

Enzyme-Linked Immunosorbent Assay and Collagen Assay

The mouse/rat HGF ELISA kit (R&D Systems, Minneapolis, MN; no. MHG00), Human/Mouse/Rat/Porcine TGF-beta 1 Quantikine ELISA Kit (R&D Systems, no. DB100B), and the Sircol Collagen Assay (Bicolor Assays, Carrickfergus, UK; no. S5000) was used according to the manufacturer's protocol.

General Animal Procedures

To induce *Sm22-Cre^{ERT}* activity, the mice were injected intraperitoneally with TAM (5 mg/30 g body weight) (Sigma no. T5648-5G).

Orthotopic Implantation

C57BL/6 mice were used for orthotopic implantation. Anesthesia of the mice was performed using medetomidine-midazolam-fentanyl (mixing ratio, 1:5:0.05 mg/mL). Primary pancreatic tumor cells with a C57BL/6 background were implanted in the tail of the pancreas; each implantation consisted of 500,000 cells in PBS (Gibco, no. 14190-094) with 10% Matrigel (Corning, no. 354230). The anesthesia was antagonized by atipamezole-flumazenil-naloxone (mixing ratio, 5:0.1:0.4).

Fluorescence-Activated Cell Sorting of Epithelial Cell Adhesion Molecule⁺ Cells Within Murine Blood Samples

Blood samples were collected by draining blood from orthotopically transplanted mice. The blood was collected in EDTA tubes. After washing the blood with DPBS, the cells were frozen in FBS with 10% dimethyl sulfoxide (Sigma, no. D2650). After thawing, the cells were washed 3 times with PBS and stained with EpCAM (eBioscience, San Diego, CA; CD326, no. 17-5791-82) and 4',6-diamidino-2-phenylindole (DAPI) (Sigma, no. D9542-1MG) in fluorescence-activated cell sorting (FACS) buffer (1 \times DPBS; 1% BSA; 1 mmol/L EDTA) for 30 minutes at 4°C. Before FACS, the cells were washed 3 times with FACS buffer and filtered through a 30- μ mol/L syringe (Filcon, Clare, MI; BD no. 340600).

Tissue Immunohistochemical Staining

Tissues were fixed in 4% PFA. Tissue processing (dehydration, embedding, and sectioning) was performed

at the Institute of Pathology, Technical University of Munich. The sections were deparaffinized by warming them up to 60°C for 15 minutes; afterward, they were immersed in xylene for 2 \times 3 minutes and afterward in alcohol, following the alcohol row from 100% to 70%. Finally, they were hydrated in water. The sections were immersed in Antigen Unmasking Solution (Vector Laboratories, Burlingame, CA; no. H-3300), according to the manufacturer's protocol. After cooling, the sections were washed with water. Endogenous peroxidase was quenched with 3% hydrogen peroxidase for 10 minutes, followed by a washing step with deionized water and PBS. The sections were blocked with Avidin D Block Reagent (Vector Laboratories, no. SP-2001), washed with PBS, and blocked again, this time with Biotin Blocking Reagent (Vector Laboratories, no. SP-2001), and washed with PBS. Afterward, the sections were blocked with Protein Blocking Agent (Thermo Fisher Scientific, StartingBlock [PBS] Blocking Buffer, no. 37538) for 10 minutes. Primary antibodies were diluted in PBT and incubated overnight. The sections were washed twice with and incubated at 37°C for 30 minutes, with secondary antibodies conjugated to biotin. Additional wash steps with PBS were performed, and then horseradish peroxidase-conjugated ABC Reagent (Vector Laboratories, no. PK-6100) was added, and the samples were incubated for 30 minutes at 37°C. Two or 3 washes with PBS were performed before developing the signal by using a DAB Substrate Kit (Vector Laboratories, no. SK-4100). The reaction was stopped with deionized water. Hematoxylin was used as a counterstain. The following antibodies were used:

- anti-fibronectin antibodies (1:200) (Abcam, Cambridge, UK; no. ab2413);
- custom rabbit anti-PRRX1A and anti-PRRX1B antibodies, generated by the Pacific Immunology Corporation (Ramona, CA);
- mouse HGF antibodies (1:200) (R&D Systems, no. AF2207);
- biotinylated goat anti-rabbit IgG antibodies (1:500, Vector Laboratories, no. BA-1000); and
- biotinylated horse anti-goat IgG antibodies (1:500, Vector Laboratories, no. BA-9500).

Picrosirius Red Staining. The sections were dewaxed and hydrated. The nuclei were stained with hematoxylin for 8 minutes and then washed under running water. The sections were stained for 1 hour in picrosirius red (0.5 g Direct Red 80; Sigma, no. 365548-5G) and 500 mL saturated aqueous solution of picric acid (Sigma, no. P6744-1GA). The sections were washed twice in acidified water (0.5% acetic acid) and dehydrated by 3 washes in 100% ethanol. The sections were rinsed with xylene and mounted.

IHC staining for immune cells was performed using a Bond RXm system (Leica, Wetzlar, Germany) with the following primary antibodies:

- anti-CD3 antibody (rabbit, 1:100) (DCS, no. CI597R0), Epitope Retrieval solution (ER) 1;
- anti-CD4 antibody (rat, 1:50) (Dianova, Hamburg, Germany; no. DIA-404), ER 2;
- anti-CD8 antibody (rat, 1:100) (Dianova, no. DIA-808), ER 1;
- anti-CD45R antibody (rat, 1:50) (BD Biosciences, Franklin Lakes, NJ; no. 553084), ER 1;
- anti-F4/80 antibody (rat, 1:50) (Bio-Rad, Hercules, CA; no. MCA497G), ER 1;
- anti-MHC II antibody (rat, 1:600) (Novus, Centennial, CO; no. M5/114.15.2), ER 1;
- anti-MPO antibody (rabbit, 1:50) (Thermo Fisher Scientific, no. RB-373-A), ER 2;
- anti-CD11b antibody (rabbit, 1:10,000) (Abcam no. ab133357), ER1; and
- rabbit anti-rat antibody (1:400) (Vector Laboratories, no. AI-4000), ER 2.

In brief, slides were deparaffinized and pretreated with ER 1 or ER 2. The following protocols were used for rabbit and rat host species:

- Host species rabbit: Primary antibody was incubated for 15 minutes at room temperature, and the antibody binding was detected with a polymer solution (8 minutes of incubation). Afterward, the antibody binding was visualized with the mixed DAB Refine solution (no. DS9800-CN, Leica), and counterstaining was performed with hematoxylin.
- Host species rat: Primary antibody was incubated for 15 minutes and the secondary rabbit-anti-rat unconjugated antibody for 30 minutes at room temperature; afterward, the polymer solution was applied (8 minutes of incubation), and antibody binding was visualized with the mixed DAB Refine solution. The counterstaining was performed with hematoxylin.

Computer-Assisted Image Analysis for the F4/80 Staining

Slides were scanned in an Aperio AT2 slide scanner (Leica) at a magnification of $\times 40$. The F4/80 expression was analyzed with Aperio ImageScope software (version 12.4.0.7018, Leica Biosystems) using the algorithm Positive Pixel Count v9, as previously described.⁶ The default set of parameters of the algorithm was modified according to the stain contrast and intensity of the scanned images. The algorithm measured the intensity of F4/80 stain (brown signal) for the whole section. The total positive pixel was normalized to the total area of the tissue section (pixel/mm²).

Tissue Immunofluorescence Staining

Paraffin-embedded sections were deparaffinized by warming them up to 60°C for 15 minutes, incubating them

with xylene (3 \times 2 minutes), 100% alcohol (2 \times 1 minutes), 96% alcohol (2 \times 1 minute), and 80% alcohol (2 \times 1 minute) and hydrating the slides by incubation in water (room temperature). The sections were immersed in Antigen Unmasking Solution (Vector Laboratories, no. H-3300) according to the manufacturer's protocol and then washed with water. Frozen sections were dried in air, fixed for 10 minutes with 4% PFA, and then rinsed in water. The sections were immersed in Antigen Unmasking Solution (Vector Laboratories, no. H-3300), and after cooling were washed with water. Afterward, the sections (paraffin-embedded sections or frozen sections) were blocked with Protein Blocking Agent (Thermo Fisher Scientific, Starting-Block [PBS] Blocking Buffer, no. 37538) for 10 minutes. The primary antibodies were diluted in PBT and were incubated with the sections overnight at 4°C in the refrigerator. The sections were washed twice with PBS and were incubated with secondary antibodies and the counterstain for 30 minutes at 37°C in the dark. The slides were washed twice with PBS and mounted with mounting media (Vector Laboratories, no. H-1200). The following antibodies were used:

- anti-smooth muscle actin antibodies (1:500) (Sigma, no. A5228),
- goat anti-type I collagen antibodies (1:250) (SouthernBiotech, Birmingham, AL; no. 1310-01),
- mouse SPARC antibodies (1:50) (R&D Systems, no. AF942),
- anti-cytokeratin 19 antibodies (1:200) (Abcam, no. 15463),
- anti-tenascin-C antibodies (1:100) (Abcam, no. ab108930),
- anti-PRRX1 antibodies (1:50) (Sigma, no. HPA051084-100UL),
- donkey anti-goat IgG 488 (1:500) (Thermo Fisher Scientific, no. A-11055),
- donkey anti-mouse IgG 647 (1:500) (Thermo Fisher Scientific, no. A-32787),
- donkey anti-rabbit IgG 595 (1:500) (Thermo Fisher Scientific, no. R37119), and
- Alexa Fluor 595 phalloidin (1:50) (Thermo Fisher Scientific, no. A12381).

Quantitative Real-Time Polymerase Chain Reaction

RNA was isolated by using a RNeasy Mini Kit (Qiagen, Hilden, Germany; no.74106). RNA (1 μ g) was transcribed into complementary DNA (cDNA) (Bioline, Memphis, TN; no. BIO-65053) and assayed by using quantitative real-time polymerase chain reaction (PCR) with a SensiFast SYBR Hi-Rox Kit (Bioline, no. BIO-92005) on the StepOnePlus System (Applied Biosystems, Foster City, CA). All experiments were performed in triplicate.

Quantitative Real-Time Polymerase Chain Reaction Primers

mPrrx1a forward: 5'-ACAGCCTCTCCGTACAGCGC-3'
 Reverse: 5'-AGTCTCAGGTTGGCAATGCT-3'
 mPrrx1b forward: 5'-CATCGTACCTCGTCTGCTC-3'
 Reverse: 5'-GCCCTCGTGTAACAACAT-3'
 mSlug forward: 5'-CCACACATTGCCTGTGTCTGCAA-3'
 Reverse: 5'-TGTGCCCTCAGGTTTGTCTGTCT-3'
 mSnail forward: 5'-ACACTGGTGAGAAGCCATTCTCCT-3'
 Reverse: 5'-TCTTCACATCCGAGTGGGTTTGGGA-3'
 mTwist forward: 5'-AGCTGAGCAAGATTAGACCCTCA-3'
 Reverse: 5'-TGCAGCTTGCCATCTTGGAGT-3'
 mVim forward: 5'-AAGACCCTGCAGTCATTCAGA-3'
 Reverse: 5'-GCAAGGATTCCACTTTCCGTTC-3'
 mZeb1 forward: 5'-TGAGCACACAGGTAAGAGGCC-3'
 Reverse: 5'-GGCTTTTCCCCAGAGTGCA-3'
 mZeb2 forward: 5'-TGATAGCCTTGCAAACCCTCTGGA-3'
 Reverse: 5'-TCCTTCATTTCTTCTGGACCGGCT-3'
 mFN1 (fibronectin) forward: 5'-ATCACAGTAGTTGCGG
 CAGGAGAA-3'
 Reverse: 5'-TGTCATAGTCAATGCCAGGCTCCA-3'
 mHgf forward: 5'-TTGGGATTGCGAGTACCCTCACAA-3'
 Reverse: 5'-TAGCCAACCTCGGATGTTTGGGTCA-3'
 mTNC forward: 5'-CCAGGGTTGCCACCTATTT-3'
 Reverse: 5'-GTCTAGAGGATCCCACTCTACTT-3'
 mPostn forward: 5'-GGTGTCTAGAAAGGATCATGG-3'
 Reverse: 5'-CAGAGCACTGGAGGGTATTTAG-3'
 mPrrx1 forward: 5'-GAAAGCAGCGGAGAAACAGGAC-3'
 Reverse: 5'-TAATCGGTTGGTCTGGGAGCAG-3'
 mActa2 forward: 5'-ACTGGGACGACATGGAAAAG-3'
 Reverse: 5'-GTTCACTGGTGCCTCTGTCA-3'

Western Blot

Western blot was performed as described previously described by Reichert et al.⁵ Anti-Prrx1 antibody (Abcam, ab211292; dilution 1:500, BD Biosciences), anti- α -SMA antibody (Cell Signaling Technology, Danvers, MA; no. 19245, dilution 1:1000) and anti- α -tubulin antibody (Sigma-Aldrich, St Louis, MO; no. T6199, dilution 1:5000) were used as primary antibodies. For detection, donkey-anti-mouse IRDye680RD (LI-COR, Lincoln, NE; no. 926-68072, dilution 1:5000) and donkey-anti-rabbit IRDye680RD (LI-COR; no. 926-68073, dilution 1:5000). Western blots were analyzed with the Odyssey Fc Dual Mode and quantified with the Image Studio Lite Software. Experiments were performed in triplicate. Error bars represent the standard error of the mean.

RNA Sequencing

Total RNA was isolated from FBs (806, PSC-3, and 699) \pm TAM treatment grown in monolayer and embedded in Matrigel with RNAeasy mini kit (Qiagen). The quality and integrity of total RNA were controlled on Agilent Technologies (Santa Clara, CA) 2100 Bioanalyzer. For RNA-seq analysis, library preparation for bulk 30-sequencing of poly(A)-RNA was done as described previously by Parekh et al.⁷ Briefly, bar-coded cDNA of each sample was generated with a Maxima RT polymerase (Thermo Fisher Scientific) using oligo-dT primer containing barcodes, unique molecular identifiers (UMIs), and

an adaptor. Fifty ends of the cDNAs were extended by a template switch oligo, and full-length cDNA was amplified with primers binding to the template switch oligo site and the adaptor. An NEB UltraII FS kit (New England Biolabs) was used to fragment cDNA. After end repair and A-tailing, a TruSeq adapter was ligated, and 3'-end fragments were finally amplified by using primers with Illumina (San Diego, CA) P5 and P7 overhangs. In comparison to Parekh et al, the P5 and P7 sites were exchanged to allow sequencing of the cDNA in read 1 and barcodes and UMIs in read 2 to achieve a better cluster recognition. The library was sequenced on a NextSeq 500 (Illumina) with 75 cycles for the cDNA in read 1 and 16 cycles for the barcodes and UMIs in read 2. Data were processed by using the published Drop-seq pipeline (v1.0) to generate sample- and gene-wise UMI tables.⁸ A reference genome (GRCm38) was used for alignment. Transcript and gene definitions were used according to the GENCODE, version M24 (www.gencodegenes.org/pages/gencode.html). All RNA-seq data are available at the European Nucleotide Archive under the accession no. PRJEB40291.

Cross-Compartment Gene Expression Correlation

Processed gene expression data for the human tumor compartment and its matched murine stroma compartment were retrieved from the supplementary material of Moffitt et al.⁹ and the website accompanying the publication from Nicolle et al.^{10,11} Raw counts from the latter were converted to transcripts per kilobase million (TPM). Fragments per kilobase million from Moffitt et al. and TPM from Nicolle et al. were log₂ transformed after adding an offset of +1. In vitro gene expression data from pancreatic stellate cells, inflammatory and myofibroblasts, respectively, as described by Öhlund et al.¹² were retrieved from the Gene Expression Omnibus (GEO) accession GSE93313. In order to examine whether there is an association between stromal Prrx1 levels and molecular subtypes of human PDAC,^{9,13,14} we first computed Pearson correlation coefficients between stromal Prrx1 and all epithelial genes in the matched datasets using the *cor.test* function from the R *stats* package. We then built a gene expression signature containing the test statistics of all epithelial genes from their respective *cor.test* outputs. Next, we applied gene set enrichment analysis¹⁵ on this signature using molecular classifier lists of PDAC as gene sets: *Classical (Collisson)*, *Quasi-mesenchymal*, *Exocrine*, *Classical (Moffitt)*, *Basal-like*, *ADEX*, *Immunogenic*, *Pancreatic Progenitor*, and *Squamous*. Results for selected classifier gene lists were illustrated by using custom R code.

Statistical Analysis of Compartment-Specific Gene Expression Data

High-throughput gene expression data from the conditions indicated in the text were carried out using the R environment for statistical computing,¹⁶ version 3.5.1.

Data Acquisition. Processed gene expression data for the human tumor compartment and its matched murine stroma compartment were retrieved from the supplement of Moffitt et al.⁹ and the website accompanying the

publication from Nicolle et al.^{10,11} Raw counts from the latter were converted to TPM. Fragments per kilobase of transcript per million mapped reads from Moffitt et al and TPM from Nicolle et al were log₂ transformed after adding an offset of +1. In vitro gene expression data from pancreatic stellate cells, inflammatory CAFs, and myofibroblasts, respectively, as described by Öhlund et al,¹² were retrieved from the GEO, accession no. GSE93313.

Cross-Compartment Correlation. To examine whether there is an association between stromal Prrx1 levels and molecular subtypes of human PDA,^{9,13,14} we first computed the Pearson correlation between stromal Prrx1 and all epithelial genes in the matched datasets using the `cor.test` function from the stats R (R Foundation for Statistical Computing, Vienna, Austria) package and built a gene expression signature containing the test statistics of all epithelial genes from their respective `cor.test` output. Next, we applied gene set enrichment analysis (GSEA)¹⁵ on this signature using molecular classifier lists of PDA as gene sets: *Classical (Collisson)*, *Quasi-mesenchymal*, *Exocrine*, *Classical (Moffitt)*, *Basal-like*, *ADEX*, *Immunogenic*, *Pancreatic Progenitor* and *Squamous*. Results for select classifier gene lists were illustrated using custom R code.

10× Genomics Single-Cell RNA-Sequencing Expression Analysis. Normalized 10× Genomics (Pleasanton, CA) murine single-cell RNA-seq data from FB-enriched fractions (DAPI⁻, CD45⁻, CD31⁻, and EpCAM⁻) of KPC tumors were obtained from GEO accession GSE129455. Annotations of ductal cells, antigen-presenting CAFs, inflammatory CAFs, and myofibroblastic CAFs, were carried out by using information from the authors.

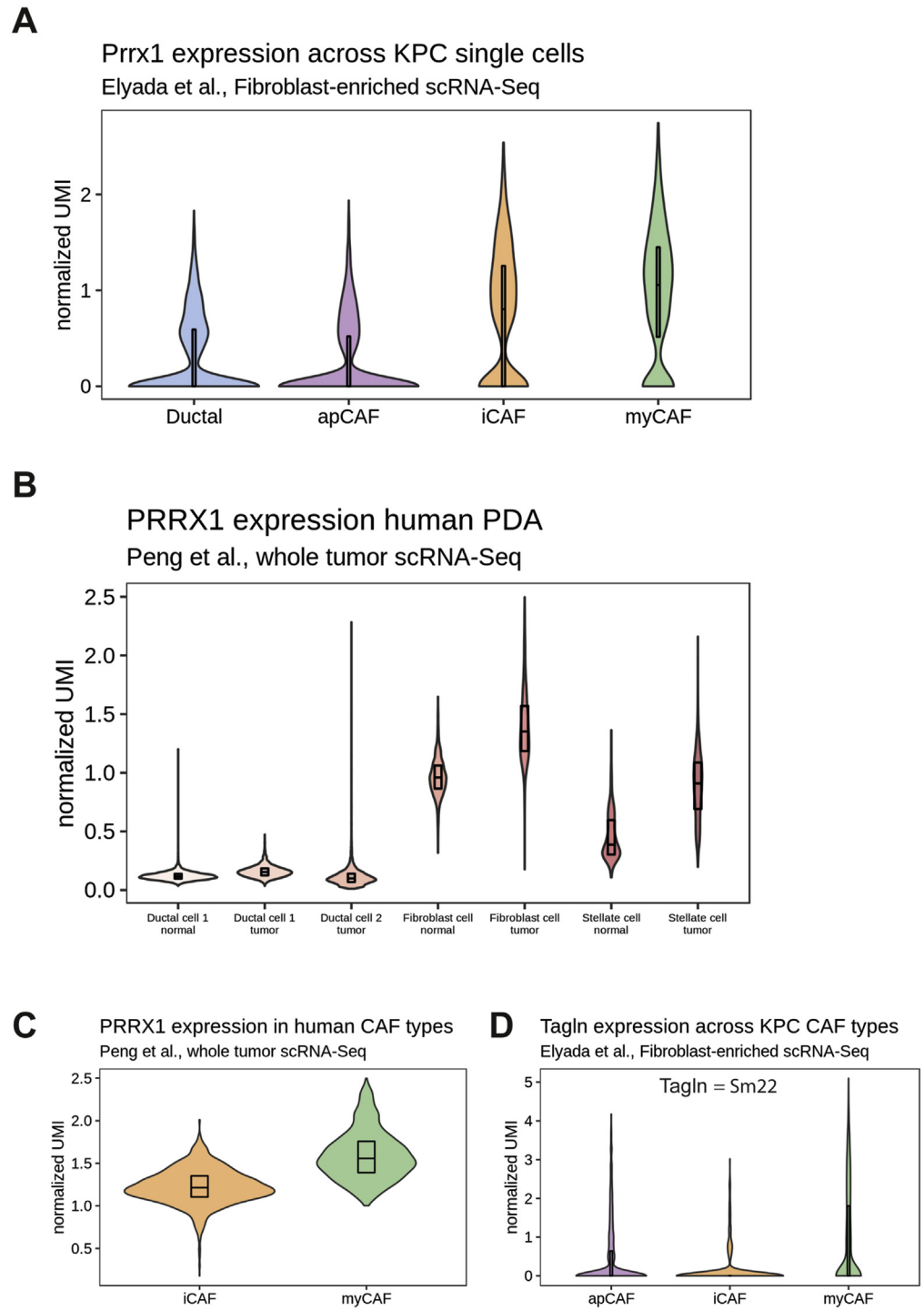
Raw UMI counts per gene and along with sample and cluster annotations of 24 human PDAC and 11 human normal pancreas samples from the study by Peng et al¹⁷ were downloaded from the Chinese National Genomics Data Center (Genome Sequence Archive accession no. CRA001160). Raw counts underwent denoising by using the provided cluster annotation and the *DCA* Python software¹⁸ and subsequent normalization using the *scrn* R package.¹⁹ Subclassification of CAFs was carried out by using human iCAF and myCAF marker genes described by Elyada et al²⁰ to carry out single-sample gene set enrichment for each of the tumor FB cells. The upper tertiles for each gene set and CAF type were isolated, with no overlap of cells, which is in line with the fundamentally different transcriptional programs between the 2 CAF populations.

Select genes (*PRRX1* for human and *Prrx1/Tagln* for murine data) and their expression levels were compared across different cell types in these single-cell RNA-seq data and tested for statistically significant differences by using the pairwise Wilcoxon function from the *Stats* R package with default settings.

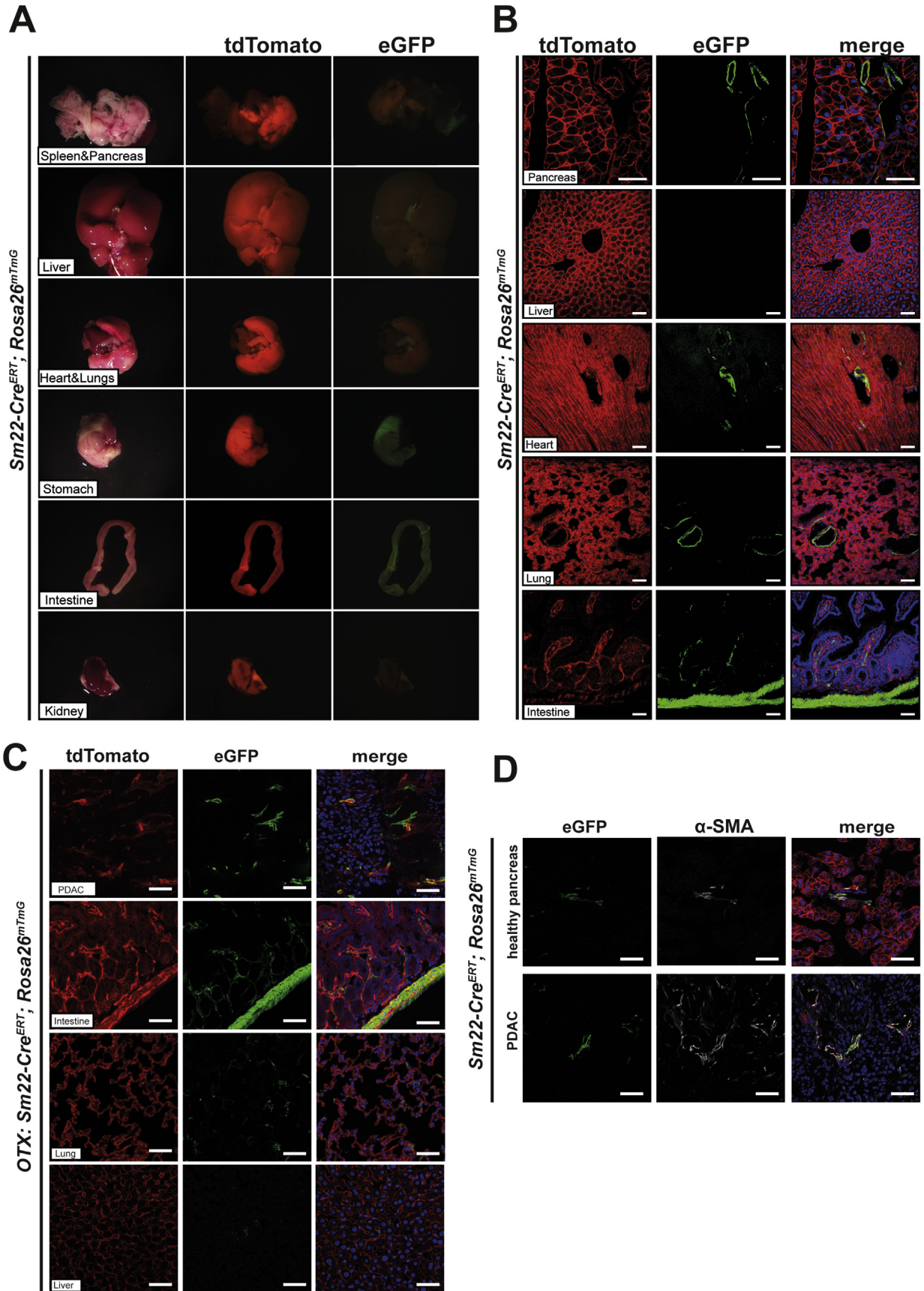
Supplementary References

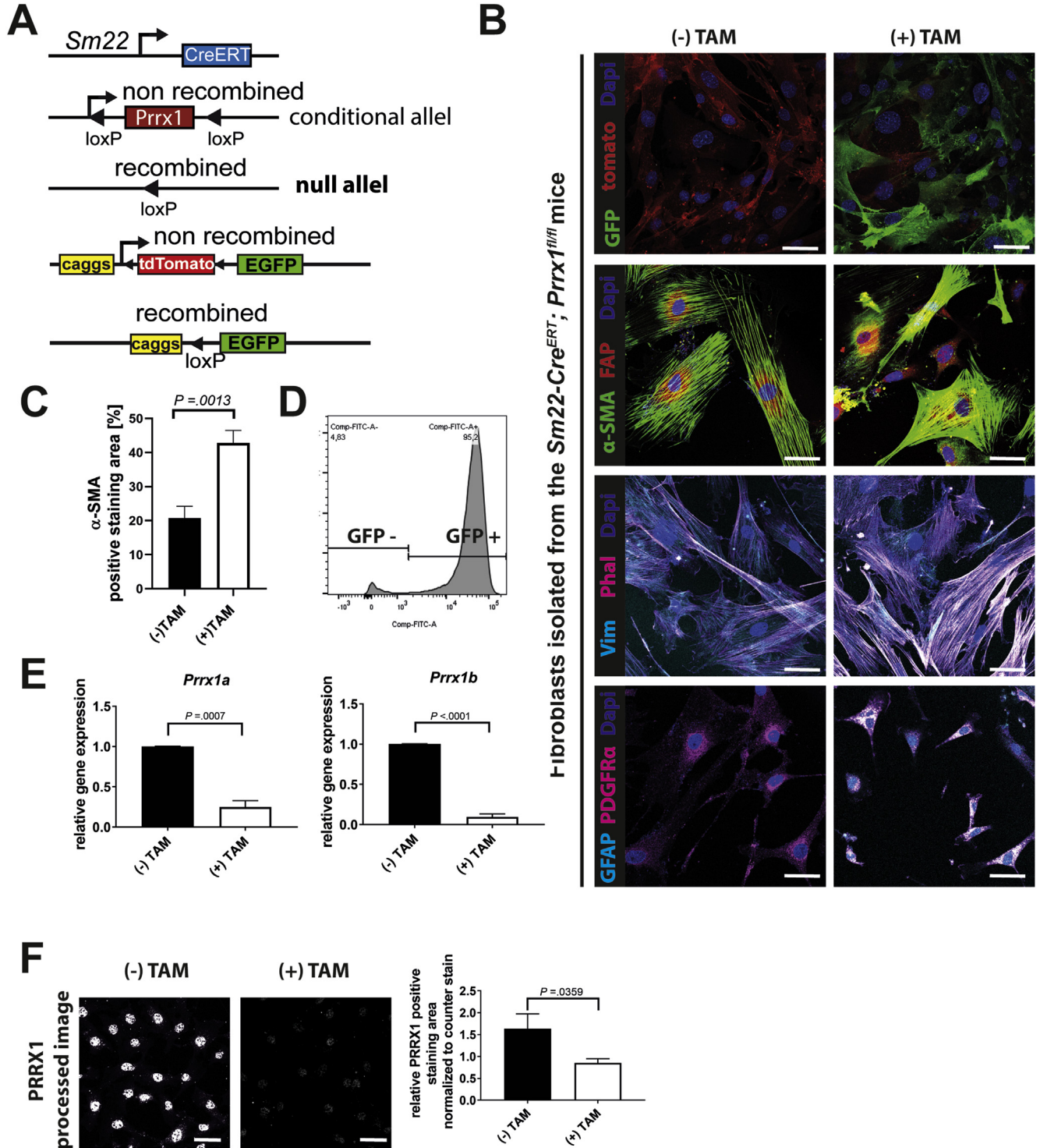
- Reichert M, Rhim AD, Rustgi AK. Culturing primary mouse pancreatic ductal cells. *Cold Spring Harb Protoc* 2015;2015:558–561.
- Vonlaufen A, Phillips PA, Yang L, et al. Isolation of quiescent human pancreatic stellate cells: a promising in vitro tool for studies of human pancreatic stellate cell biology. *Pancreatology* 2010;10:434–443.
- Demir IE, Boldis A, Pfitzinger PL, et al. Investigation of Schwann cells at neoplastic cell sites before the onset of cancer invasion. *J Natl Cancer Inst* 2014;106(8):dju184.
- Böttcher RT, Veelders M, Rombaut P, et al. Kindlin-2 recruits paxillin and Arp2/3 to promote membrane protrusions during initial cell spreading. *J Cell Biol* 2017;216:3785–3798.
- Reichert M, Takano S, von Burstin J, et al. The Prrx1 homeodomain transcription factor plays a central role in pancreatic regeneration and carcinogenesis. *Genes Dev* 2013;27:288–300.
- Brazdziute E, Laurinavicius A. Digital pathology evaluation of complement C4d component deposition in the kidney allograft biopsies is a useful tool to improve reproducibility of the scoring. *Diagn Pathol* 2011;6(Suppl 1):S5.
- Parekh S, Ziegenhain C, Vieth B, et al. The impact of amplification on differential expression analyses by RNA-seq. *Sci Rep* 2016;6:25533.
- Evan, Basu A, Satija R, et al. Highly parallel genome-wide expression profiling of individual cells using nanoliter droplets. *Cell* 2015;161:1202–1214.
- Moffitt RA, Marayati R, Flate EL, et al. Virtual microdissection identifies distinct tumor- and stroma-specific subtypes of pancreatic ductal adenocarcinoma. *Nat Genet* 2015;47:1168–1178.
- Nicolle R, Blum Y, Marisa L, et al. Pancreatic adenocarcinoma therapeutic targets revealed by tumor-stroma cross-talk analyses in patient-derived xenografts. *Cell Rep* 2017;21:2458–2470.
- Nicolle R, Iovanna J. PaCaOmicsDATA.
- Öhlund D, Handly-Santana A, Biffi G, et al. Distinct populations of inflammatory fibroblasts and myofibroblasts in pancreatic cancer. *J Exp Med* 2017;214:579–596.
- Collisson EA, Sadanandam A, Olson P, et al. Subtypes of pancreatic ductal adenocarcinoma and their differing responses to therapy. *Nat Med* 2011;17:500–503.
- Bailey P, Chang DK, Nones K, et al. Genomic analyses identify molecular subtypes of pancreatic cancer. *Nature* 2016;531(7592):47–52.
- Subramanian A, Tamayo P, Mootha VK, et al. Gene set enrichment analysis: a knowledge-based approach for interpreting genome-wide expression profiles. *Proc Natl Acad Sci U S A* 2005;102:15545–15550.
- R Core Team. R: a language and environment for statistical computing. Vienna, Austria, 2018.
- Peng J, Sun B-F, Chen C-Y, et al. Single-cell RNA-seq highlights intra-tumoral heterogeneity and malignant progression in pancreatic ductal adenocarcinoma. *Cell Res* 2019;29:725–738.
- Eraslan G, Simon LM, Mircea M, et al. Single-cell RNA-seq denoising using a deep count autoencoder. *Nat Commun* 2019;10(1):390.

- 19. Lun ATL, McCarthy DJ, Marioni JC. A step-by-step workflow for low-level analysis of single-cell RNA-seq data with Bioconductor. *F1000Res* 2016; 5:2122.
- 20. Elyada E, Bolisetty M, Laise P, et al. Cross-species single-cell analysis of pancreatic ductal adenocarcinoma reveals antigen-presenting cancer-associated fibroblasts. *Cancer Discov* 2019;9:1102–1123.



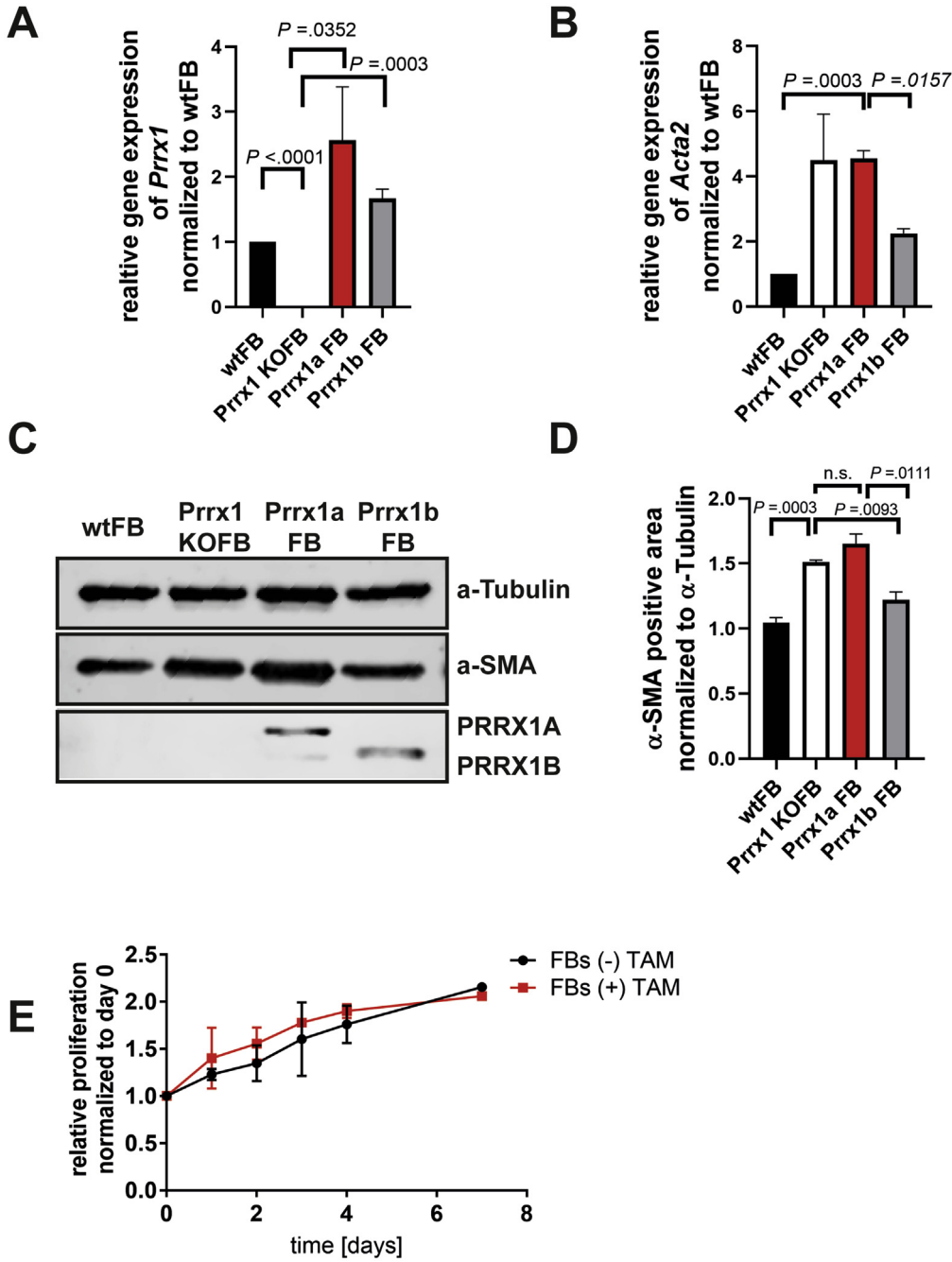
Supplementary Figure 1. *Prrx1* expression in different CAF entities based on single-cell RNA-seq data. Statistics are shown in [Supplementary Tables 2–5](#). (A) Violin plot showing the *Prrx1* expression across KPC single cells for ductal, apCAFs, iCAFs, and myCAFs. (B) Violin plot showing the *PRRX1* expression in human PDA. (C) Violin plot showing the *PRRX1* expression in human CAF subtypes. (D) Violin plot showing the *Tagln* expression in murine CAF entities. scRNA, small conditional RNA.



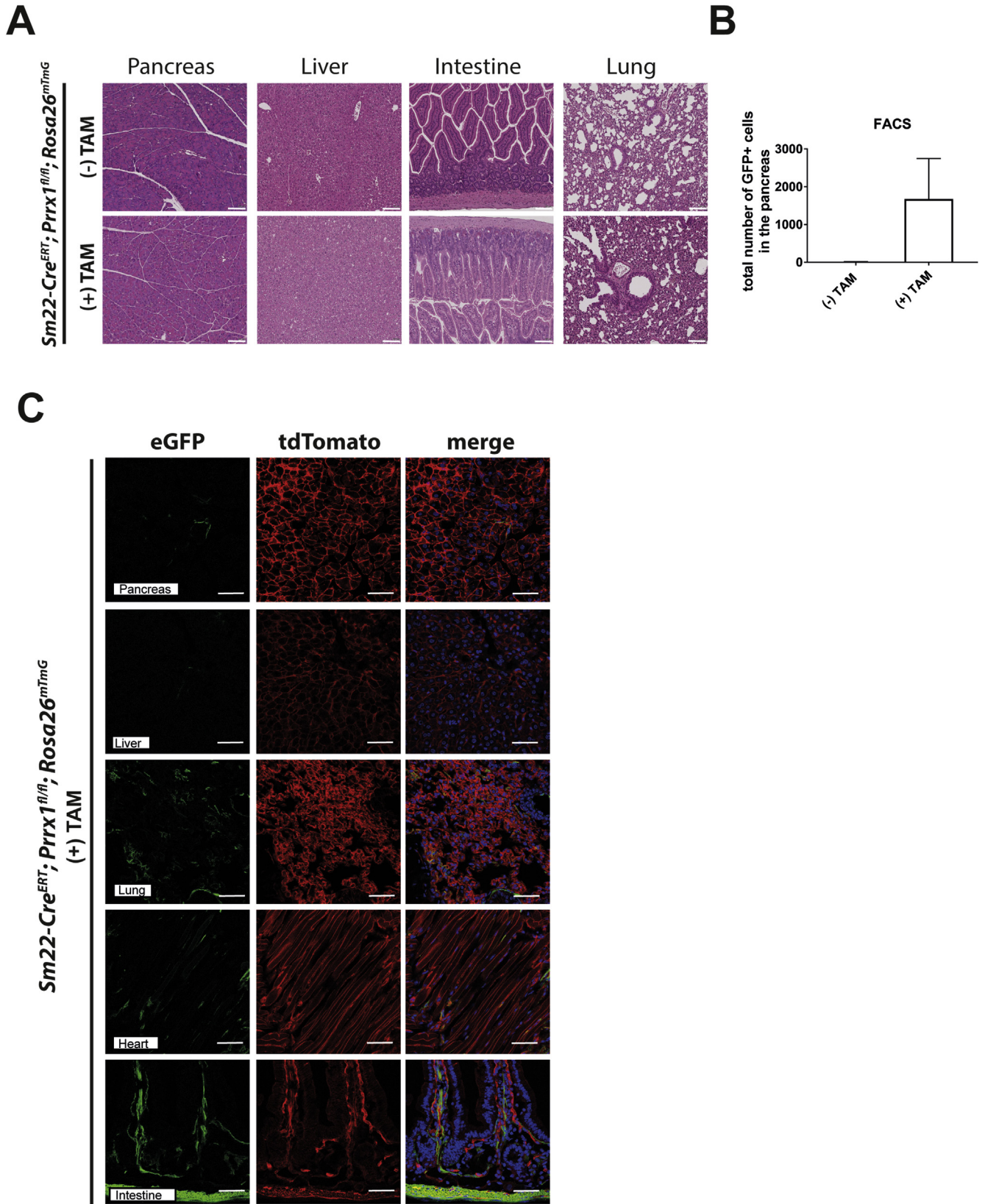


Supplementary Figure 3. Characterization of *Sm22-Cre^{ERT};Prrx1^{fl/fl}* FBs in vitro. (A) Schematic illustration of the genetic background of the used mouse model. (B) Representative IF staining of isolated FBs; scale bar, 50 μ m. (C) Semiquantitative image processing was used to quantify the α -SMA staining; unpaired Student *t* test. (D) FACS analysis of isolated FB cell lines after 4 days of TAM treatment, sorting of GFP⁺ (fluorescein isothiocyanate) cells. (E) Quantitative PCR analysis of *Prrx1a* and *Prrx1b* expression levels in primary murine cell lines; unpaired Student *t* test. (F) Semiquantitative processed image of the PRRX1 staining, quantification of the PRRX1 positive staining area normalized to the nuclear counter stain; unpaired Student *t* test.

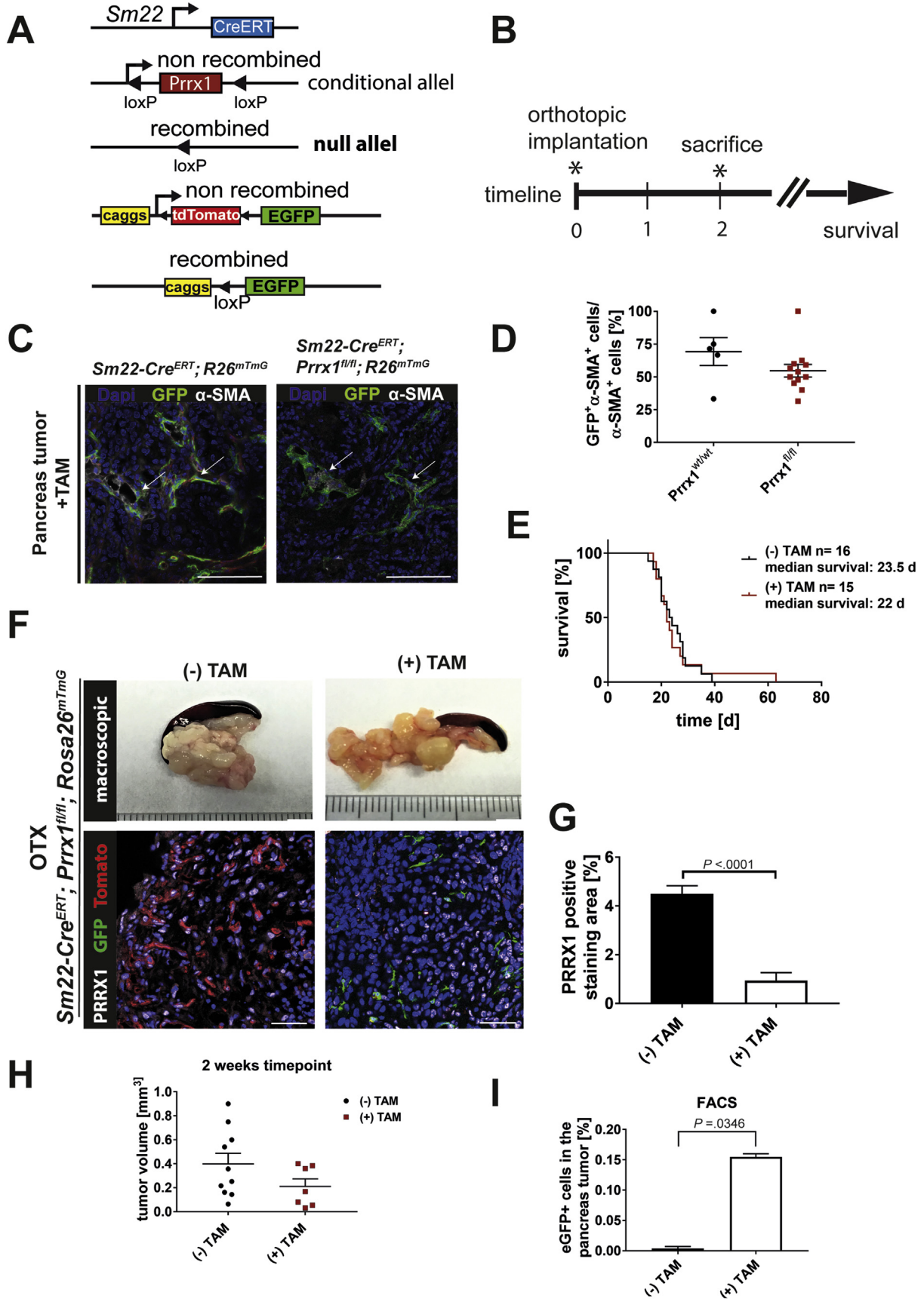
Supplementary Figure 2. Characterization of the *Sm22-Cre^{ERT};R26^{mTmG}* expression pattern. (A) Left row: macroscopic picture of the organs (spleen and pancreas, liver, heart and lungs, stomach, intestine, kidney) taken with the Zeiss (Oberkochen, Germany) Stemi 11 fluorescence stereomicroscope. Middle and right rows: macroscopic IF pictures of the organs with the endogenous signal *R26^{mTmG}* expression pattern, tdTomato (red) and eGFP (green). (B) Representative IF pictures of the microscopic expression pattern of the *Sm22-Cre^{ERT};R26^{mTmG}*, DAPI (blue), tdTomato (red), and eGFP (green); scale bar, 50 μ m. (C) Orthotopic implantation of the 8025 PDAC cell line into the pancreas tail; representative IF pictures for each organ: DAPI (blue), tdTomato (red), and eGFP (green); scale bar, 50 μ m. (D) Representative IF pictures of pancreas and PDAC showing the overlap of α -SMA- (white) and eGFP- (green) positive cells; DAPI staining (blue); scale bar, 50 μ m.



Supplementary Figure 4. Rescue of Prrx1-knockout FBs by Prrx1 isoform-specific over-expression. (A) Quantitative PCR analysis of *Prrx1a* and *Prrx1b* expression in primary murine embryonic FBs; unpaired Student *t* test. (B) Quantitative PCR analysis of *Acta2* expression in primary murine embryonic FBs; unpaired Student *t* test. (C) Representative Western blot of α -tubulin, α -SMA, PRRX1A, and PRRX1B. (D) Quantification of the α -SMA positive area (Western blot) with Image Studio Lite, version 5.2; unpaired Student *t* test. (E) Proliferation assay (MTT) of the *Sm22-Cre^{ERT};Prrx1^{fl/fl}* FBs was performed over 8 days.

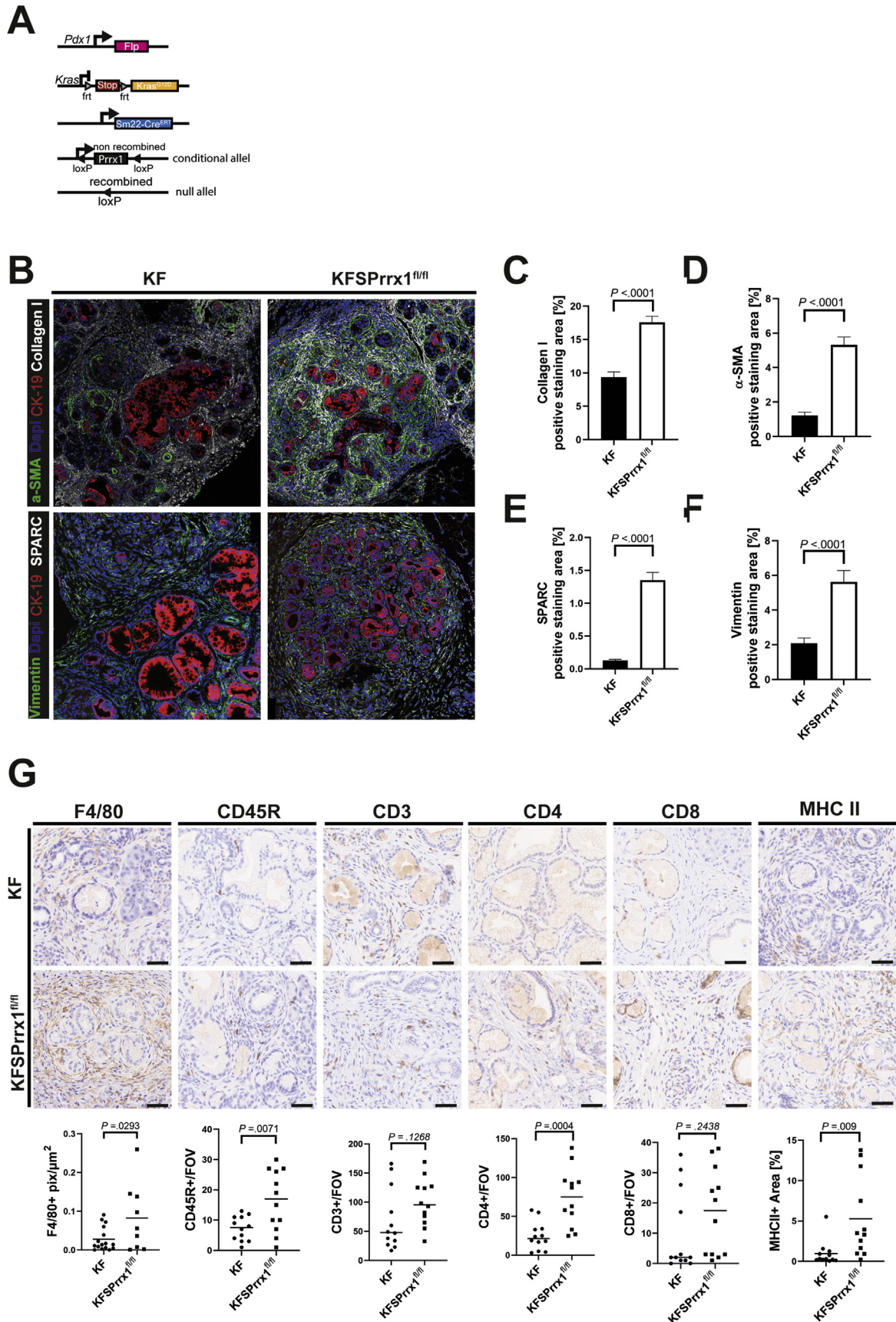


Supplementary Figure 5. Altering *Prrx1* levels of *Sm22-Cre^{ERT}*-positive FBs in healthy tissue. (A) Representative H&E staining of pancreas, liver, lung, and intestine of 3-month-old mice; n = 3 per group; scale bar, 100 μ m. (B) FACS of GFP⁺ cells of the entire pancreas; n = 3 per group. (C) Representative IF image of cryosection with endogenous tdTomato (red) and eGFP (green) signal; counterstain with DAPI; scale bar, 50 μ m.

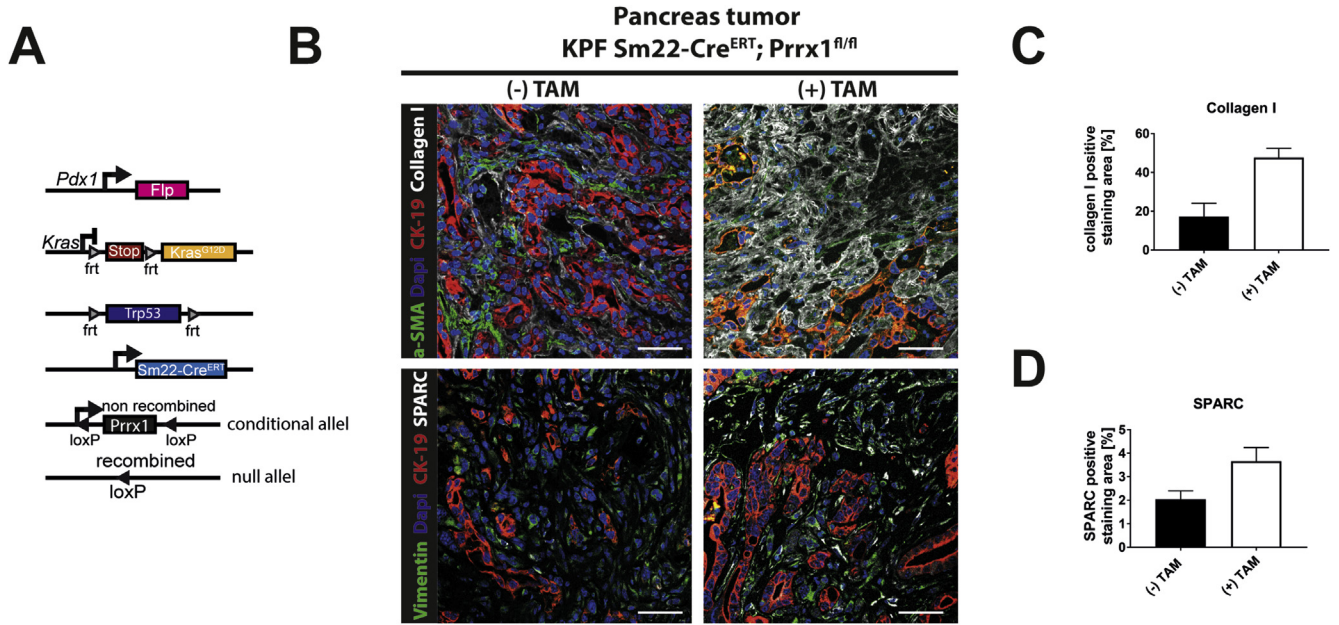


←

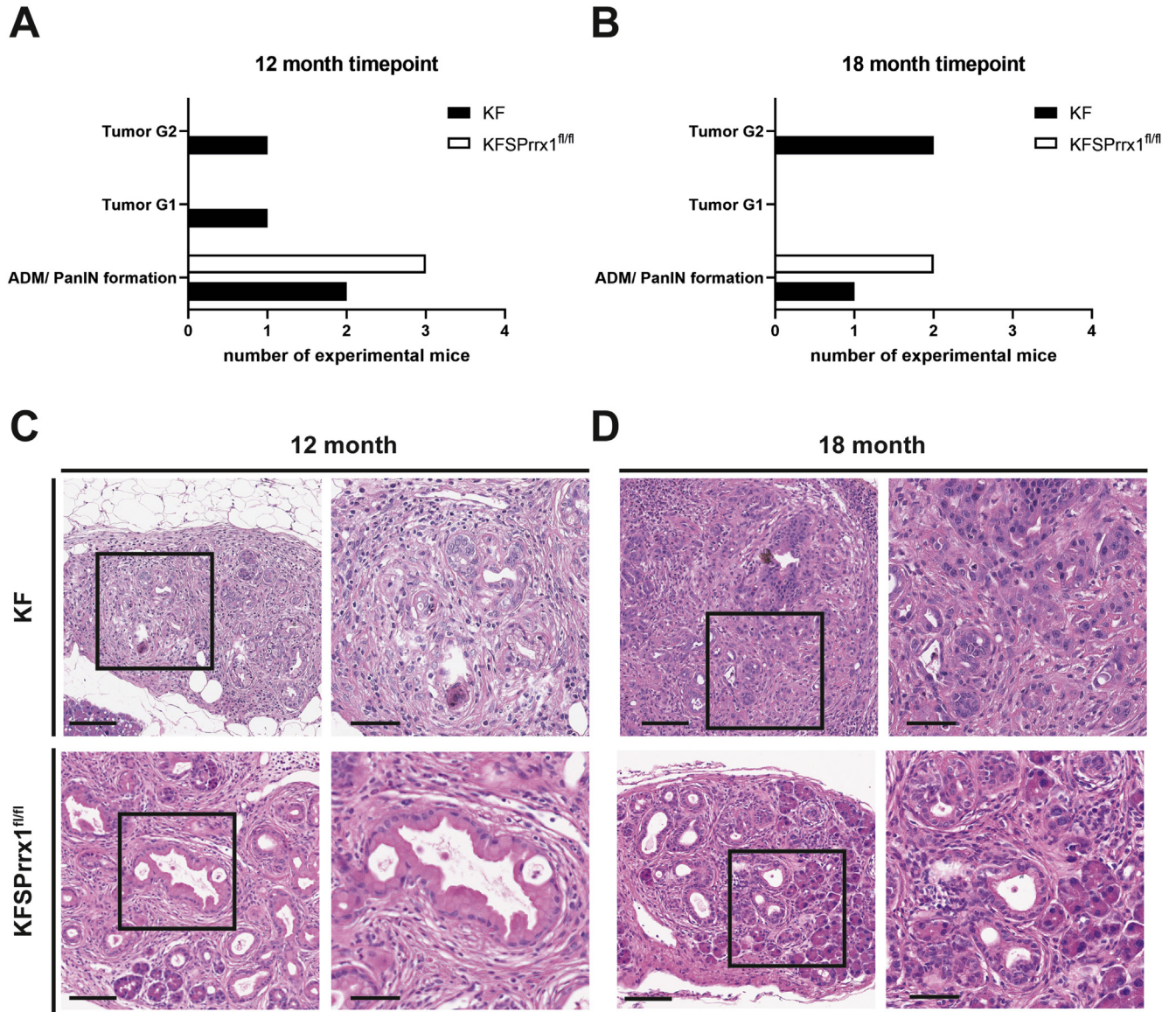
Supplementary Figure 6. Altering *Prrx1* levels of *Sm22-Cre^{ERT}*-positive FBs in the orthotopic implantation model. (A) Schematic illustration of the mouse model used for orthotopic implantation. (B) Schematic illustration showing the experimental design of the orthotopic implantation experiment with the *p48-Cre;LSL-Kras^{G12D}* (8025) cell line. (C) Compartment-specific recombination of *Prrx1*; IF staining of pancreatic tumor for α -SMA (*white*), endogenous signal for eGFP (*green*), and tdTomato (*red*), with nuclear counterstain (*blue*, DAPI); arrows indicate double-positive cells for α -SMA and eGFP. (D) Manually counted eGFP- and α -SMA-positive cells per field of view. (E) Kaplan-Meier survival curves of *Sm22-Cre^{ERT};Prrx1^{fl/fl}* treated and untreated with TAM. (F) Upper row: Macroscopic picture of the pancreas tumor. Lower row: Representative IF image of cryosection with endogenous tdTomato (*red*) and eGFP (*green*) signal; PRRX1 (*white*) staining and counterstain with DAPI (*blue*); scale bar, 50 μ m. (G) Semiquantitative image processing was used to quantify the PRRX1 staining. Unpaired Student *t* test; *****P* < .0001. (H) Tumor volume of the 2-week timepoint. (-) TAM, n = 10; (+) TAM, n = 7. (I) FACS analysis of the pancreas tumor; sorting of the eGFP+ population.



Supplementary Figure 7. ECM remodeling in the *KFSPrrx1^{fl/fl}* mouse model. (A) Schematic illustration of the endogenous *KFSPrrx1^{fl/fl}* mouse model. (B) Immunofluorescence analysis of the *KF* and *KFSPrrx1^{fl/fl}* mouse model at the 12-month timepoint. Upper row: Representative IF staining for CK-19, DAPI; collagen; α -SMA, scale bar = 50 μ m; lower row: representative IF staining for CK-19, DAPI; SPARC; vimentin, scale bar = 50 μ m scale bar. (C) Semiquantitative image processing was used to quantify collagen I staining, unpaired Student *t* test. (D) Semiquantitative image processing was used to quantify α -SMA staining; unpaired Student *t* test. (E) Semiquantitative image processing was used to quantify SPARC staining; unpaired Student *t* test. (F) Semiquantitative image processing was used to quantify vimentin staining, unpaired Student *t* test. (G) Immunohistologic analysis of pancreatic tumor stromal changes in the *KF* and *KFSPrrx1^{fl/fl}* mouse model at the 12-month timepoint; representative stainings for macrophages (F4/80), B cells (CD45R), T cells (CD3), T helper cells (CD4), cytotoxic T cells (CD8), and dendritic cells (MHC II); scale bar, 100 μ m. Data were analyzed by using an unpaired Student *t* test. FOV, field of view.

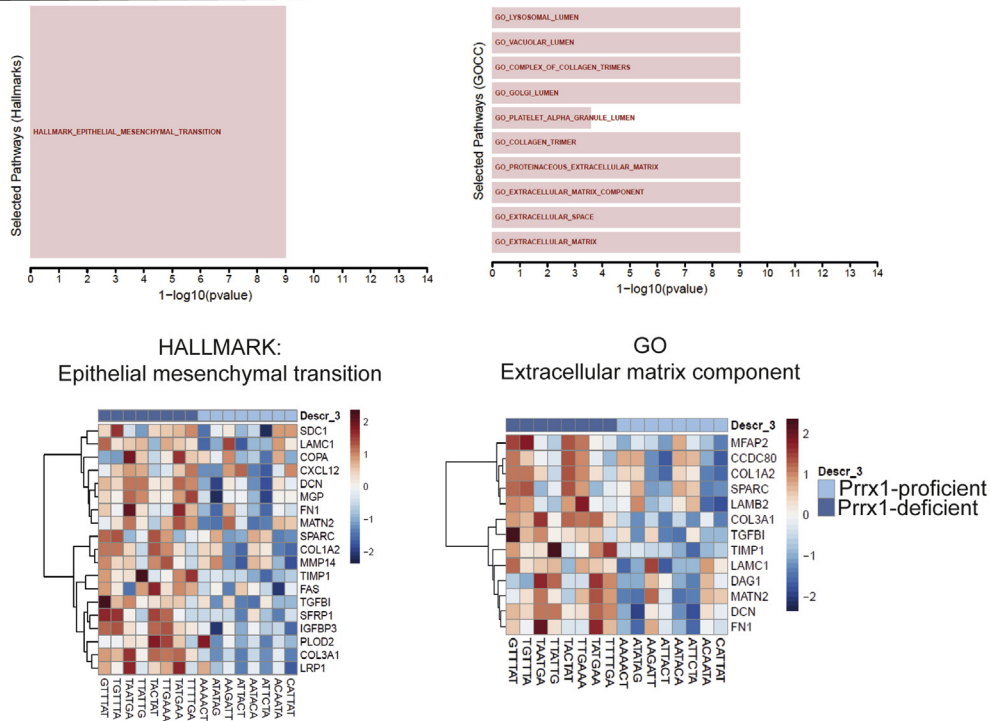


Supplementary Figure 8. ECM remodeling in the *KPF Sm22-Cre^{ERT2}; Prrx1^{fl/fl}* model. (A) Schematic illustration of the endogenous mouse model. (B) Upper row: Representative IF staining for CK-19, DAPI, collagen, and α -SMA; scale bar, 50 μ m. Lower row: representative IF staining for CK-19, DAPI, SPARC, and vimentin; scale bar, 50 μ m. (C) Semiquantitative image processing was used to quantify collagen I staining; unpaired Student *t* test. (D) Semiquantitative image processing was used to quantify SPARC staining; unpaired Student *t* test.

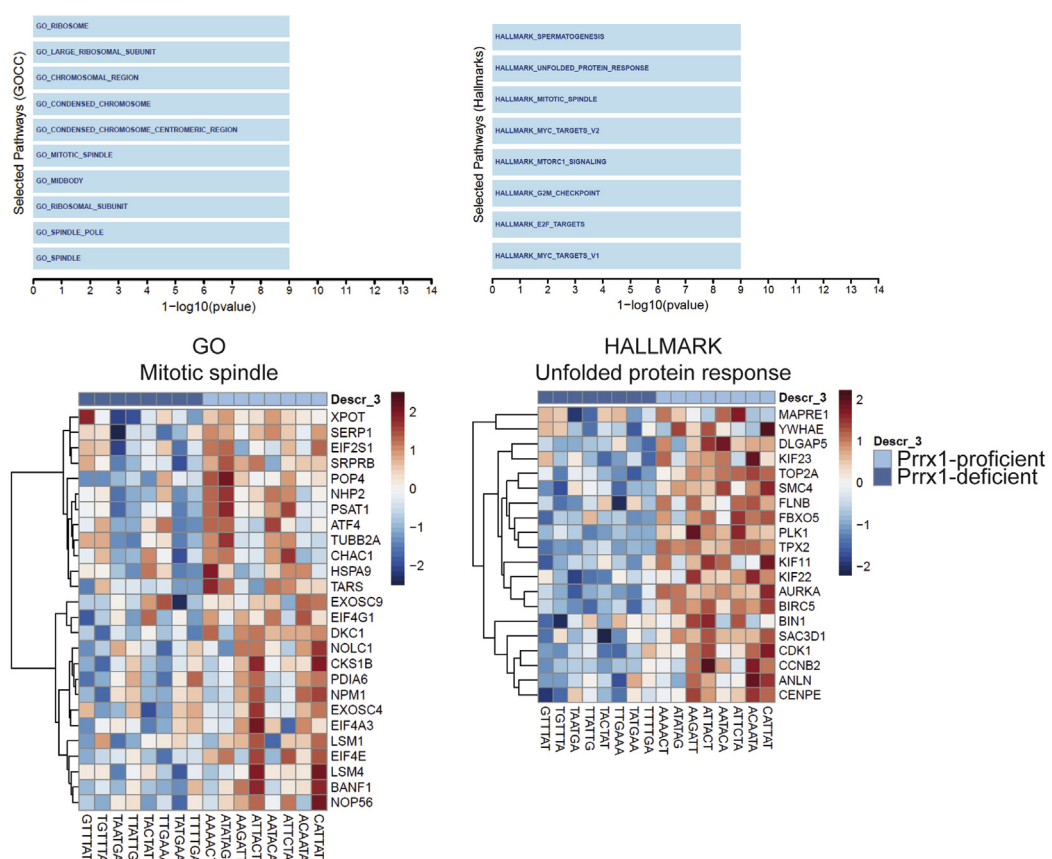


Supplementary Figure 9. Histopathologic analysis of the *KF* and *KFSPrrx1^{fl/fl}* mouse model. (A) Histologic grading of the *KF* and *KFSPrrx1^{fl/fl}* mouse model at the 12-month timepoint. (B) Histologic grading of the *KF* and *KFSPrrx1^{fl/fl}* mouse model at the 18-month timepoint. (C) Histopathologic analysis of the pancreas at the 12-month timepoint; scale bars, 100 μ m and 50 μ m. (D) Histopathologic analysis of the pancreas at the 18-month timepoint; scale bars, 100 μ m and 50 μ m.

A Enriched genesets in *Prrx1*-deficient fibroblasts



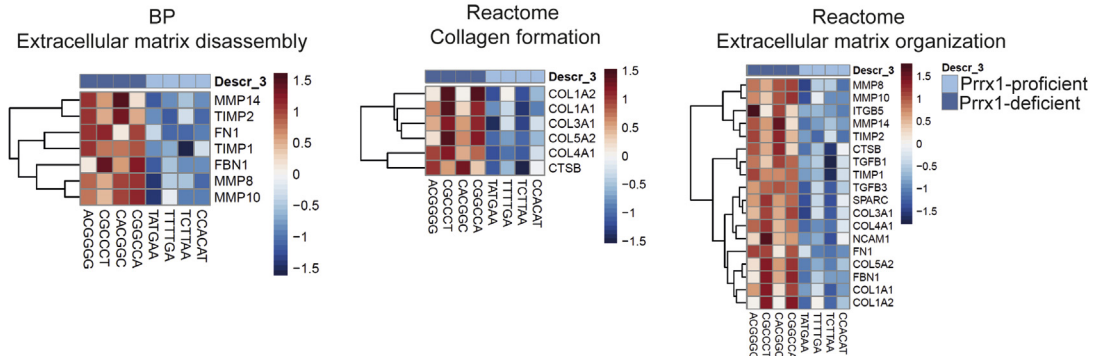
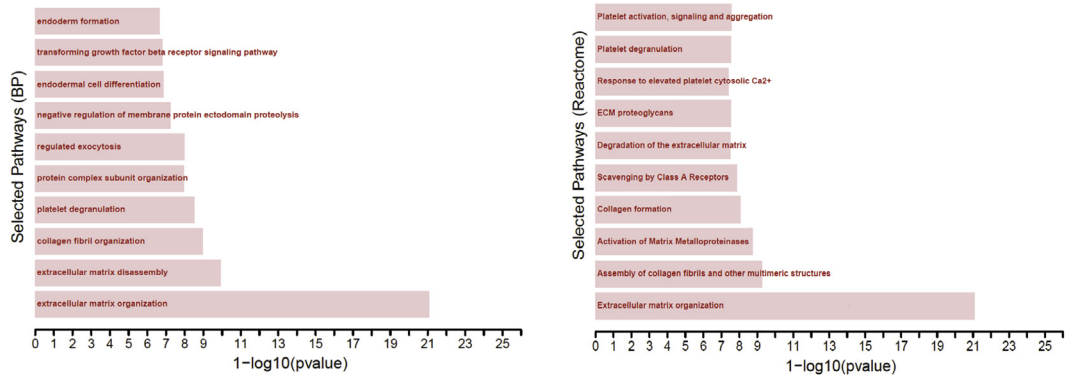
B Enriched genesets in *Prrx1*-proficient fibroblasts



Supplementary Figure 10. Prrx1-deficient and -proficient FBs have different transcriptional programs. RNA-seq analysis of *Prrx1*-proficient and *Prrx1*-deficient (TAM treated) FBs grown in a monolayer (cell lines, n = 4; technical replicates, n = 4). (A) The bar diagram shows significant enriched gene sets for *Prrx1*-deficient FBs. The heatmap shows differentially expressed genes between *Prrx1*-proficient and -deficient FBs for different gene sets. (B) The bar diagram shows significant enriched gene sets for *Prrx1*-proficient FBs. The heatmap shows differentially expressed genes between *Prrx1*-proficient and -deficient FBs for different gene sets. GO, Gene Ontology.

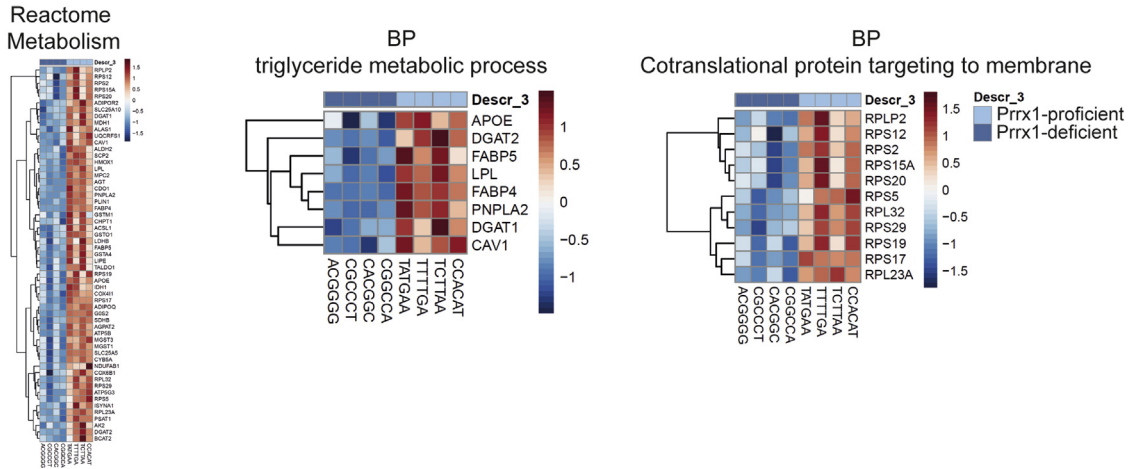
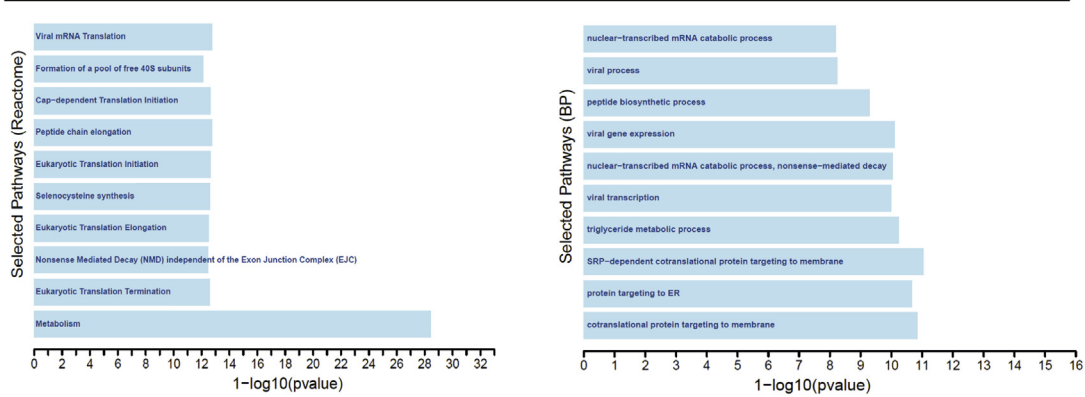
A

Enriched genesets in *Prrx1*-deficient fibroblasts grown in 3D



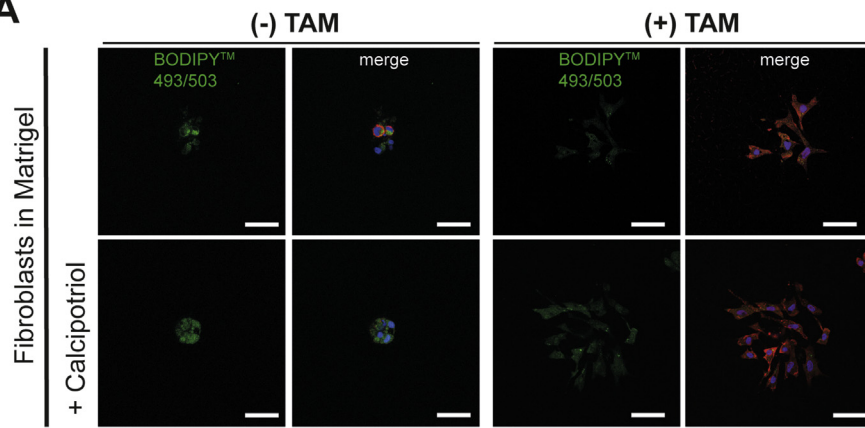
B

Enriched genesets in *Prrx1*-proficient fibroblasts grown in 3D

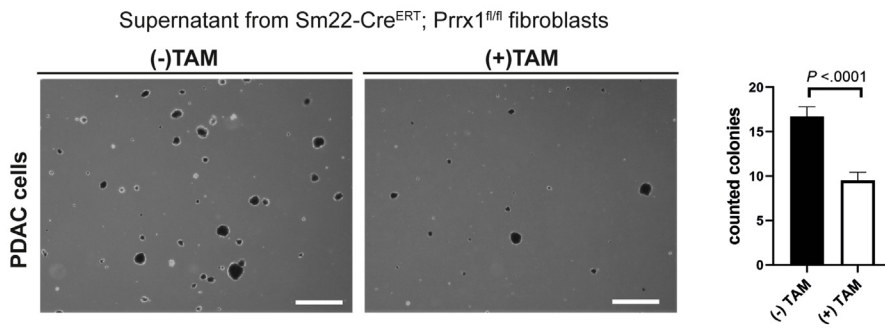


Supplementary Figure 11. Prrx1-deficient FBs cannot revert into a quiescent state embedded in Matrigel. RNA-seq analysis of *Prrx1*-proficient and *Prrx1*-deficient (TAM treated) FBs embedded in Matrigel (cell lines, n = 2; technical replicates, n = 4). (A) The bar diagram shows significant enriched gene sets for *Prrx1*-deficient FBs. The heatmap shows differentially expressed genes between *Prrx1*-proficient and -deficient FBs for different gene sets. (B) The bar diagram shows significant enriched gene sets for *Prrx1*-proficient FBs. The heatmap shows differentially expressed genes between *Prrx1*-proficient and -deficient FBs for different gene sets. BP, biological processes.

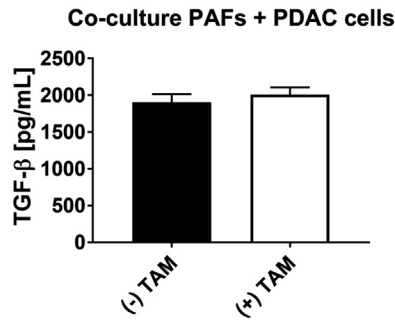
A



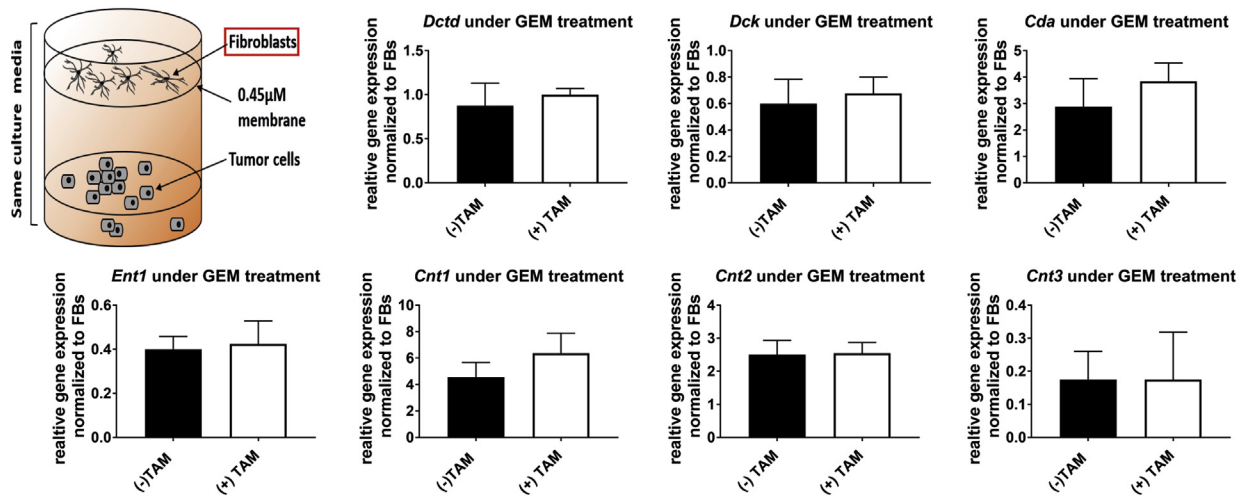
B



C



D



Supplementary Figure 12. *Prrx1* alters the plasticity of FBs, the anchorage-independent growth of tumor cells, but does not influence gemcitabine metabolism. (A) Primary murine FBs embedded in Matrigel were treated or not treated with 100 nmol/L calcipotriol for 48 hours, fixed, and stained with BODIPY 493/503 (*green*) for the detection of neutral lipids, phalloidin (*red*), and DAPI (*blue*). BODIPY (Thermo Fisher Scientific, Waltham, MA; no. D3922) 493/503-positive cells contain cytoplasmic lipid droplets, a hallmark of the quiescent state. (B) Soft agarose assay of PDAC cells cultured with the supernatant of *Prrx1*-proficient and -deficient FBs. Supernatant from 3 different FB cell lines were used, and the colony formation was counted manually; unpaired Student *t* test. (C) TGF- β ELISA of the supernatant of tumor cells cocultured with FB in a Transwell. Three different FB cell lines were used. (D) Schematic illustration of the Transwell coculture experiment analyzing the FBs. Quantitative PCR analysis of gemcitabine metabolism (gemcitabine transporters and inactivating enzymes) expressed in FBs cocultured with tumor cells under gemcitabine (600 nmol/L, 72 hours). M, mol/L.

Supplementary Table 1.List of All Primary Cell Lines Used In the Experiments

Name	Genetic background	Organism	Cell type
PSC-1	<i>Sm22-Cre^{ERT};Prrx1^{fl/fl};R26^{mTmG}</i>	<i>Mus musculus</i>	Pancreatic stellate cells
PSC-3	<i>Sm22-Cre^{ERT};Prrx1^{fl/fl};R26^{mTmG}</i>	<i>Mus musculus</i>	Pancreatic stellate cells
806	<i>Sm22-Cre^{ERT};Prrx1^{fl/fl};R26^{mTmG}</i>	<i>Mus musculus</i>	Pancreatic stellate cells
K212	<i>Sm22-Cre^{ERT};Prrx1^{fl/fl}</i>	<i>Mus musculus</i>	Pancreatic FBs
K337	<i>Sm22-Cre^{ERT};Prrx1^{fl/fl}</i>	<i>Mus musculus</i>	Pancreatic FBs
K338	<i>Sm22-Cre^{ERT};Prrx1^{fl/fl}</i>	<i>Mus musculus</i>	Pancreatic FBs
K699	<i>Sm22-Cre^{ERT};Prrx1^{fl/fl}</i>	<i>Mus musculus</i>	Pancreatic FBs
K704	<i>Sm22-Cre^{ERT};Prrx1^{fl/fl}</i>	<i>Mus musculus</i>	Pancreatic FBs
GK5471 FB	<i>Pdx1-Cre;Kras^{G12D/+}</i>	<i>Mus musculus</i>	PanIN FBs
AK2055FB	<i>Pdx1-Cre;Kras^{G12D/+}</i>	<i>Mus musculus</i>	PanIN FBs
AK1872FB	<i>Pdx1-Cre;Kras^{G12D/+}</i>	<i>Mus musculus</i>	PanIN FBs
AK1998	<i>Pdx1-Cre;Kras^{G12D/+}</i>	<i>Mus musculus</i>	PanIN cells
GK5377	<i>Pdx1-Cre;Kras^{G12D/+};R26^{mTmG}</i>	<i>Mus musculus</i>	PanIN cells
GK5407	<i>Pdx1-Cre;Kras^{G12D/+};R26^{mTmG}</i>	<i>Mus musculus</i>	PanIN cells
8025	<i>p48-Cre;LSL-Kras^{G12D/+}</i>	<i>Mus musculus</i>	PDAC cells
SB1560	<i>p48-Cre;LSL-Kras^{G12D/+};Tgfb2^{fl/fl}</i>	<i>Mus musculus</i>	Pancreatic CAFs
hPCa2		Human	PDAC cells
hPCa3		Human	PDAC cells
PDO-B34		Human	PDAC cells
hPCaFB outgrowth		Human	Pancreatic CAFs
hPCaFB outgrowth 2		Human	Pancreatic CAFs
hPSC		Human	Pancreatic stellate cells
hPCaFB 2655		Human	Pancreatic CAFs
wtFB		<i>Mus musculus</i>	Embryonic FBs
Prrx1 KOFB	Global <i>Prrx1</i> knockout	<i>Mus musculus</i>	Embryonic FBs
Prrx1a FB	Global <i>Prrx1</i> knockout, stable transduced with <i>pTRIPz-Prrx1a</i>	<i>Mus musculus</i>	Embryonic FBs
Prrx1b FB	Global <i>Prrx1</i> knockout, stable transduced with <i>pTRIPz-Prrx1b</i>	<i>Mus musculus</i>	Embryonic FBs
PDC 1	<i>C57BL/6</i> mice	<i>Mus musculus</i>	Pancreatic ductal cells
PDC 2	<i>C57BL/6</i> mice	<i>Mus musculus</i>	Pancreatic ductal cells
PDC 3	<i>C57BL/6</i> mice	<i>Mus musculus</i>	Pancreatic ductal cells
FB1	<i>C57BL/6</i> mice	<i>Mus musculus</i>	FBs
FB2	<i>C57BL/6</i> mice	<i>Mus musculus</i>	FBs
FB2	<i>C57BL/6</i> mice	<i>Mus musculus</i>	FBs

Supplementary Table 2. Statistical Analyses of the Violin Blot “Prrx1 Expression Across KPC Single Cells” by Comparing Group 1 With Group 2

Group 1	Group 2	Family-wise error rate
apCAF	Ductal	0.00267343
iCAF	Ductal	5.57E-81
myCAF	Ductal	4.644E-186
iCAF	apCAF	1.4711E-77
myCAF	apCAF	1.931E-156
myCAF	iCAF	6.9421E-18

Supplementary Table 4. Statistical Analyses of the Violin Blot “Prrx1 Expression in Human CAF Types” by Comparing Group 1 With Group 2

Group1	Group2	Family-wise error rate
myCAF	iCAF	<0.001

Supplementary Table 3. Statistical Analyses of the Violin Blot “Prrx1 Expression Human PDA” by Comparing Group 1 with Group 2

Group 1	Group 2	FWER
Ductal cell 1 tumor	Ductal cell 1 normal	<0.001
Ductal cell 2 tumor	Ductal cell 1 normal	7.582E-134
FB cell normal	Ductal cell 1 normal	<0.001
FB cell tumor	Ductal cell 1 normal	<0.001
Stellate cell normal	Ductal cell 1 normal	<0.001
Stellate cell tumor	Ductal cell 1 normal	<0.001
Ductal cell 2 tumor	Ductal cell 1 tumor	<0.001
FB cell normal	Ductal cell 1 tumor	<0.001
FB cell tumor	Ductal cell 1 tumor	<0.001
Stellate cell normal	Ductal cell 1 tumor	5.199E-276
Stellate cell tumor	Ductal cell 1 tumor	<0.001
FB cell normal	Ductal cell 2 tumor	<0.001
FB cell tumor	Ductal cell 2 tumor	<0.001
Stellate cell normal	Ductal cell 2 tumor	<0.001
Stellate cell tumor	Ductal cell 2 tumor	<0.001
FB cell tumor	FB cell normal	<0.001
Stellate cell normal	FB cell normal	7.048E-196
Stellate cell tumor	FB cell normal	5.1075E-12
Stellate cell normal	FB cell tumor	<0.001
Stellate cell tumor	FB cell tumor	<0.001
Stellate cell tumor	Stellate cell normal	5.327E-201

Supplementary Table 5. Statistical Analyses of the Violin Blot “Tagln Expression Across KPC CAF Types” by Comparing Group 1 With Group 2

Group1	Group2	FWER
iCAF	apCAF	1.7122E-30
myCAF	apCAF	1.1889E-17
myCAF	iCAF	6.2281E-94